Persistent dopamine-dependent remodeling of the neural transcriptome in response to pregnancy and postpartum

Jennifer C Chan[1], Giuseppina Di Salvo[1,2], Ashley M Cunningham[1], Sohini Dutta[1], Elizabeth A Brindley[1], Ethan Wan[4], Cindy Zhang[1], Ian Maze[1,3,5*]

Affiliations

[1]Nash Family Department of Neuroscience, Friedman Brain Institute, Icahn School of Medicine at Mount Sinai, New York, NY, 10029, USA

[2]Department of Psychiatry and Neuropsychology, School for Mental Health and Neuroscience (MHeNs), Maastricht University, Maastricht, The Netherlands

[3]Department of Pharmacological Sciences, Icahn School of Medicine at Mount Sinai, New York, NY, 10029, USA

[4]Department of Neurobiology, University of Alabama at Birmingham, Birmingham, AL 35294, USA.

[5]Howard Hughes Medical Institute, Icahn School of Medicine at Mount Sinai, New York, NY, 10029, USA

***Corresponding author**
Ian Maze
Email: ian.maze@mssm.edu

SUMMARY

Pregnancy and postpartum experiences represent transformative physiological states that impose lasting demands on the maternal body and brain, resulting in lifelong neural adaptations. However, the precise molecular mechanisms driving these persistent alterations remain poorly understood. Here, we used brain-wide transcriptomic profiling to define the molecular landscape of parity-induced neural plasticity, identifying the dorsal hippocampus (dHpc) as a key site of transcriptional remodeling. Combining single-cell RNA sequencing with a maternal-pup separation paradigm, we additionally demonstrated that chronic postpartum stress significantly disrupts dHpc adaptations by altering dopamine dynamics, leading to dysregulated transcription, altered cellular plasticity, and impaired behavior. We further established the sufficiency of dopamine modulation in the regulation of these parity-induced adaptations via chemogenetic suppression of dopamine release into dHpc, which recapitulated key transcriptional and behavioral features of parity in virgin females. In sum, our findings establish dopamine as a central regulator of parity-induced neuroadaptations, revealing a fundamental transcriptional mechanism by which female reproductive experiences remodel the maternal brain to sustain long-term behavioral adaptations.

INTRODUCTION

Matrescence – the physical, emotional, hormonal, and social transition to motherhood – is a period of profound transformation that reshapes the maternal body and brain to support pregnancy, birth, and offspring care. While extensive research has focused on acute maternal brain processes that are essential for the onset and maintenance of parenting, how precisely brain adaptations are sustained beyond the postpartum period to persistently influence behavior remains unclear. Recent human neuroimaging studies have revealed that pregnancy experience induces long-lasting alterations in brain connectivity and structure, persisting for years or even decades following birth[1–6]. Animal models examining parity – the state of previously carrying a pregnancy to term – similarly have demonstrated persistent alterations in synaptic remodeling, cell proliferation, and behavioral outcomes[7–14]. However, the specific mechanisms within the extensive repertoire of maternal physiological changes that drive these long-lasting brain adaptations remain poorly understood. With over 130 million pregnancies occurring globally each year, elucidating how female reproductive experiences shape long-term brain plasticity remains a fundamental question with widespread clinical implications. Given that parity may modulate risk and/or resilience to certain neurological and neuropsychiatric disorders[15–17], addressing this gap in knowledge will be essential for advancing our understanding of maternal brain health.

Here, we began by employing brain-wide transcriptional profiling to systematically characterize the persistent impact of parity on the maternal brain in mice, which provided important insights into the regulation of signaling pathways and cellular compositions across maternal circuits. These analyses surprisingly revealed the dorsal hippocampus (dHpc) as a key site of sustained plasticity. We then leveraged single-cell RNA sequencing, a postpartum stress paradigm, behavioral assays, and chemogenetic approaches to identify and validate a dopamine-dependent neuromodulatory

process that orchestrates these sustained maternal adaptations. Importantly, these brain-wide datasets will also serve as a critical resource for future investigations into the reproductive state-dependent adaptations that contribute to matrescence.

RESULTS

Parity promotes long-lasting transcriptional and behavioral adaptations in maternal brain

To first investigate the persistent effects of female reproductive experiences in maternal brain, we established a timeline to compare primiparous dams (PP), which experienced breeding, pregnancy, parturition, lactation, and pup interactions, to age-matched virgins that lacked reproductive experiences (nulliparous, NP; **Fig. 1A**). Given that reproductive hormones return to baseline levels ~7-weeks post-conception[18], we then conducted brain-wide transcriptomic profiling 4-weeks following cessation of pup rearing (10-weeks post-conception; i.e. 49 days postpartum; dpp), as this time point would be predicted to reflect sustained changes. Following differential expression analyses of the 11 brain regions selected based on prior evidence supporting their involvement in maternal behaviors[19,20] (**Fig. S1A**), our data revealed a wide-range in the number of differentially expressed genes (DEGs, adj. $p < 0.05$) across brain regions (**Fig. 1B, Table S1**). These differences indicated varying levels of transcriptomic sensitivity to parity brain-wide, with few changes observed in the medial prefrontal cortex (mPFC), for example, as compared to the dHpc, the region that was found to be most robustly regulated in our analyses.

To next assess whether these differential expression patterns could be attributed to changes in shared cell-types, we performed cell-type deconvolution using BRETIGEA, which compares whole transcriptome data to validated brain cell type-specific marker gene sets[21]. We observed changes in cell marker expression for neurons, astrocytes, microglia, oligodendrocyte precursor

92 cells (OPCs), oligodendrocytes, and endothelial cells across brain regions, regardless of the
93 number of DEGs (except for mPFC; **Fig. 1C**). These data suggested that cellular changes may
94 occur across brain regions independently of the extent of transcriptomic alterations, potentially
95 reflecting shifts in the proportion of neurons to non-neuronal/glial cells, modifications in synaptic
96 plasticity, or changes in cell identity in response to prior reproductive experiences. Notably, the
97 expression of neuronal markers was found to be downregulated in brain regions displaying the
98 most DEGs (**Fig. 1C**). Furthermore, a significant inverse correlation between reduced neuronal
99 marker expression and the number of DEGs across all brain regions implicated changes in neuronal
100 populations that may underlie the observed transcriptional responses (**Fig. 1D**); note that this
101 relationship was not observed for other cell-types (**Fig. S1B-F**). These findings nicely align with
102 human neuroimaging studies, which have reported reduced gray matter in mothers even years after
103 birth, a phenomenon that has been proposed to refine maternal neural circuits to optimize
104 caregiving behavior[1,2,4,22].
105
106 Based on these findings, we hypothesized that such shared neuronal marker alterations may
107 indicate common upstream mechanisms driving regional-specific transcriptional responses. To test
108 this, we first compared DEGs across brain regions to identify common gene sets that were altered
109 by parity status, which led to the observation that the greatest extent of overlap occurs in those
110 regions displaying the highest levels of transcriptional sensitivity (**Fig. 1E**). Based on these
111 analyses, we then grouped the 11 brain regions according to the number of DEGs, the degree of
112 overlap with other regions, and significant fold changes in neuronal marker expression, based on
113 the premise that these regions may be co-regulated to elicit convergent transcriptional responses
114 to parity (referred to as "high sensitivity" regions: dHpc, nucleus accumbens (NAc), medial
115 preoptic area (mPOA), locus coeruleus (LC), ventral hippocampus (vHpc)). Brain regions lacking

116 these criteria were classified as "low sensitivity" regions (dorsal raphe nucleus (DRN),
117 paraventricular nucleus of the hypothalamus (PVN), basolateral amygdala (BLA), ventral
118 tegmental area (VTA), olfactory bulb (OB), mPFC). Next, we explored the predicted upstream
119 regulators of overlapping DEGs in "High" versus "Low" sensitivity brain regions, which revealed
120 several upstream regulators that were grouped into common molecular classes, including
121 hormones, neurotransmitter/neurotrophin signaling molecules, transcriptional regulators, and
122 others (**Fig. 1F**). While both High and Low sensitivity regions were found to share upstream
123 regulators within these molecular classes, High sensitivity regions displayed greater enrichment
124 for estrogen, progesterone, testosterone, dopamine, and other ligands with similar receptor affinity
125 or structural homology. In contrast, regulators that were classified within the lipid category were
126 uniquely associated with Low sensitivity regions.
127
128 To further explore the regulatory networks that distinguish High versus Low sensitivity regions,
129 we performed weighted gene co-expression network analysis (WGCNA) across all 11 brain
130 regions[23], resulting in nine co-expression modules (**Fig. S1G-J**). Module-trait correlations, in
131 which the trait refers to a combination of group (NP *vs.* PP) and regional sensitivity (High *vs.*
132 Low), identified significant correlations between High sensitivity regions in PP females and the
133 brown, green, yellow, and magenta modules (**Fig. 1G;** henceforth labeled 'parity-sensitive
134 modules'). To identify the specific brain regions exhibiting changes in module gene expression,
135 we then examined enrichment of DEGs within each module, with an extended focus on the parity-
136 sensitive modules. Consistent with our module-trait correlational analysis, parity-sensitive
137 modules displayed significant enrichment for DEGs from dHpc (**Fig. 1H;** Fisher's exact tests:
138 brown, $p < 10^{-16}$; green, yellow, $p < 10^{-6}$), NAc (brown, green, $p < 10^{-3}$; magenta, $p < 0.01$; yellow,
139 $p < 0.05$), mPOA (green, $p < 0.05$; magenta, $p < 0.01$), LC (magenta, $p < 0.05$), and vHpc (magenta,

140 $p < 0.05$; yellow, $p < 0.01$). Functional annotation analysis of the genes from these modules
141 highlighted their significant enrichment in signaling pathways related to neuromodulators, such as
142 estrogen (yellow, brown) and dopamine (green, magenta), in agreement with our upstream
143 regulator analyses (**Fig. 1I, Fig. S1K-L**). In contrast, Low sensitivity regions were found to be
144 significantly associated with the black module, which was enriched for genes associated with RNA
145 and macromolecule processing pathways (**Fig. 1G, 1I**).
146
147 Building on these transcriptomic findings, we next investigated whether parity leads to sustained
148 functional alterations in PP females. To evaluate the extent of such persistence, we performed
149 behavioral assessments at 140 dpp, ~16-weeks after pup weaning (**Fig. 1A**). Behavioral tasks were
150 selected to specifically assess functions associated with the brain regions displaying robust
151 transcriptional changes, including maternal behavior, learning, and memory. To assess maternal
152 behavior, we tested pup retrieval in the home cage by placing two donor pups in opposite corners
153 away from the nest. PP dams were observed to retrieve pups with significantly reduced latency as
154 compared to NP females (**Fig. 1J**), which is consistent with previous findings, though at a more
155 extended timepoint in our studies[24]. Next, to investigate the functional impact of dHpc
156 transcriptional changes, we utilized a contextual fear conditioning paradigm. Female mice were
157 habituated to the training context before receiving five shocks (2-seconds each, 0.7 mA) with 90-
158 second intertrial intervals. Both NP and PP females demonstrated significant training acquisition,
159 as indicated by increased freezing compared to no-shock controls (**Fig. 1K**). Notably, PP females
160 exhibited enhanced acquisition, with significantly increased freezing observed by the third shock,
161 while NP females only displayed significant freezing at the fifth shock (**Fig. 1K**). During the
162 context test conducted 24-hours later, both groups demonstrated recall, with PP females showing
163 higher freezing responses than NP animals (**Fig. 2L**). Given the involvement of these brain regions

164 in anxiety- and depressive-like behaviors, we also assessed affective phenotypes using the open
165 field, light-dark box, and forced swim tests, however, no significant differences were observed
166 (**Fig. S2A-H**). These results suggested that the transcriptional changes observed in parity-sensitive
167 brain regions may promote maternal and dHpc-related behavioral outcomes, as has been reported
168 previously[7,10,12,14,25–31], though the mechanisms underlying such prolonged functional adaptations
169 remained unclear. To account for the potential influence of estrous cycling on behavioral changes,
170 vaginal swabs were collected immediately following testing, and behavioral analyses were
171 stratified by estrous stage. No significant effects of estrous stage were observed (**Fig. S2I-N**),
172 thereby supporting parity status as the primary driver of the observed behavioral differences.
173
174 ***Pregnancy and postpartum experiences promote persistent maternal neuroplasticity***
175 Since our paradigm comparing NP *vs.* PP females could not distinguish between the discrete
176 reproductive event(s) that may be responsible for the sustained transcriptional alterations observed,
177 we next sought to isolate those key events throughout the female reproductive window. To do so,
178 we compared females that were successfully bred to males but did not become pregnant (Mating
179 Only), females that experienced pregnancy and parturition but did not transition to postpartum due
180 to pup removal on the day of birth (Pregnancy Only), and virgin females exposed to 21-days of
181 donor pup interactions (Pup Sensitized). These groups were analyzed in parallel with age-matched
182 NP and PP females to delineate the contributions of specific reproductive and maternal experiences
183 (**Fig. 2A**). Consistent with previous studies[32], four days of pup exposures sensitized virgin females
184 to maternal behavior, as evidenced by increased crouching over pups and decreased pup avoidance
185 by day 4 (**Fig. S3A**). To determine the processes conferring sustained transcriptional sensitivity,
186 we focused our investigations on the dHpc due to its pronounced gene expression response to
187 parity. When comparing NP *vs.* PP gene expression profiles, we observed that the Pregnancy Only

188 group most closely resembled that of the expression profile of PP females, suggesting that
189 pregnancy is a primary driver of dHpc neuroplastic changes (**Fig. 2B, Fig. S3B**). However, the
190 magnitude of fold changes did not match that of the PP group, indicating that additional
191 experiences, likely during postpartum, are also necessary to fully establish parity-induced changes
192 in the dHpc.
193
194 While visualization of differential expression profiles in the Mating Only and Pup Sensitized
195 groups did not mimic PP changes, comparisons to NP did identify significant DEGs across all
196 groups, with the most substantial changes observed in the Pup Sensitized group, followed by the
197 Pregnancy Only, and Mating Only groups (**Fig. S3C-E, Table S2**). Overlapping DEGs induced
198 by discrete reproductive events significantly intersected with DEGs in PP animals, again
199 suggesting that while pregnancy is the primary driver of parity-induced effects, each reproductive
200 event contributes, in part, to this process (**Fig. S3F**). Next, we overlapped DEGs from each
201 comparison with genes from parity-sensitive modules (from **Fig. 1**) to assess the contribution of
202 each reproductive event to parity programming. Significant overlap was observed across all
203 groups, with Pregnancy Only and Pup Sensitized groups displaying the strongest enrichment,
204 indicating that these experiences play a key role in shaping persistent dHpc alterations (**Fig. 2C**).
205 Thus, despite the lack of similarity between the overall expression profiles between Pup Sensitized
206 *vs.* PP, gene expression changes induced by pup interactions likely converge on similar regulatory
207 networks, albeit through different DEGs, which are critical for parity-driven transcriptional
208 alterations. To further explore these relationships, we performed threshold-free Rank-Rank
209 Hypergeometric Overlap (RRHO) analyses[33], which demonstrated transcriptional concordance
210 across experiences, with the strongest overlap observed in pregnancy (**Fig. 2D**). These findings
211 suggest that reproductive exposures converge, or act additively, to drive the full extent of brain

212 transcriptional changes. Furthermore, comparing GO term analyses of DEGs for each group
213 revealed significant enrichment in overlapping biological processes, with many related to synaptic
214 signaling and plasticity pathways (**Fig. 2E**). Notably, certain pathways were unique to the
215 combination of reproductive exposures, including changes in CREB activity, catecholamine
216 secretion, and myelination, indicating that these regulatory processes depend on multiple
217 reproductive events to achieve full induction (**Fig. 2E**). Although this study did not address the
218 specific contributions of parturition or lactation, our findings demonstrate that pregnancy
219 establishes the foundation for parity-induced transcriptional alterations in dHpc, with additional
220 postpartum exposures also required to fully promote these responses.
221
222 Given that postpartum experiences enhanced changes that were initiated during pregnancy, we
223 conducted a controlled time course study to examine these transcriptional dynamics across
224 gestational and postpartum periods in age-matched females (**Fig. 2F**). Pregnancy timepoints were
225 selected to represent the anabolic and catabolic phases of gestation, corresponding to early (7.5
226 days post-conception, dpc) and late (17.5 dpc) stages, respectively. Postpartum timepoints were
227 chosen to capture the immediate effects of hormonal withdrawal following parturition (2 dpp), as
228 well as a later stage prior to pup weaning (21 dpp). Based on the hypothesis that parity-induced
229 transcriptional alterations are progressively enhanced across reproductive stages, we first
230 compared DEGs at each timepoint (*vs.* NP) to genes from parity-sensitive modules identified
231 previously. DEGs from all comparisons significantly overlapped with the brown module (**Fig. 2G,**
232 **left; Table S3**), suggesting that pathways enriched in this module are central to dHpc
233 programming. Enrichment in the green and yellow modules was predominantly found to be
234 induced by postpartum exposures, potentially amplifying the effects of the pathways driven by the
235 brown module (**Fig. 2G, left**). To assess the regional specificity of these dynamic changes, we

236 analyzed bulk RNA-seq data from the vHpc, a region that displayed moderate sensitivity to parity
237 status (**Fig. 2G, middle; Table S4**), along with the mPFC, which exhibited few transcriptional
238 alterations (**Fig. 2G, right; Table S5**). These regions exhibited limited overlap of DEGs with
239 parity-sensitive module genes, further emphasizing the specificity of the pathways that drive long-
240 term adaptations in brain regions displaying heightened sensitivity to parity.
241
242 To then characterize cumulative transcriptional changes that occur across reproductive stages, we
243 performed a time course analysis using the ImpulseDE2 package to detect genes displaying
244 sustained or transient expression alterations[34]. This analysis revealed a prominent set of genes that
245 displayed persistent and progressive downregulation, with more pronounced alterations during
246 postpartum (**Fig. 2H**). These genes were significantly enriched for processes related to
247 glutamatergic synapses, dopaminergic signaling, and endocrine-related pathways (**Fig. 2I**).
248 Conversely, genes with persistent upregulation were found to be enriched for pathways associated
249 with cell junction dynamics (**Fig. 2J**), which is consistent with overall prolonged changes in
250 synaptic plasticity and transmission. Additionally, we identified gene sets displaying transient
251 alterations, including downregulation of neurogenesis-related pathways, and upregulation of
252 copper ion metabolism (**Fig. 2K-L**); these data are consistent with other studies reviewed here[35,36].
253 In total, these findings highlight postpartum as a key window for reinforcing parity-induced
254 alterations.
255
256 ***Chronic maternal stress during postpartum disrupts dHpc adaptations***
257 We next examined whether postpartum perturbations may disrupt pathways that reinforce parity-
258 induced alterations in dHpc. As becoming a new parent represents a significant source of stress,
259 we implemented a maternal stress paradigm that robustly increases stress hormone levels and

260 disrupts key postpartum experiences, including nursing and pup interactions, from 10–20 dpp (**Fig.**
261 **3A, Fig. S3G**). During this period, dams were separated from their pups for 3-hours daily and were
262 provided with limited nesting materials until pup weaning (Stress PP). As litter size represents a
263 potential confounding factor, the time period selected reduces the impact of maternal stress on pup
264 mortality that can occur immediately following birth. By 10 dpp, pups were more durable, as
265 reflected by the absence of litter size differences between Control and Stress dams (**Fig. S3H**).
266 Accordingly, no differences in postpartum weights were observed, suggesting that this postpartum
267 stress paradigm does not induce major metabolic alterations in the dams (**Fig. S3I**). To assess the
268 extent of parity adaptations in Stress PP, we compared this group to NP and Control PP animals.
269 Principal components analysis (PCA) of dHpc transcriptional profiles revealed distinct clustering
270 of NP and Control PP groups (reproducing our prior analyses), while Stress PP samples were found
271 to cluster intermediately between the two groups (**Fig. 3B**). Similarly, hierarchical clustering of all
272 DEGs resulted in intermingling of NP and Stress PP samples (**Fig. 3C, Table S6**), suggesting that
273 postpartum stress disrupts the extent of parity alterations in dHpc. To determine whether genes
274 induced by parity are reversed by stress, we then compared DEGs with opposing directionality in
275 NP *vs.* Control PP and Control PP *vs.* Stress PP groups (**Fig. 3D**). Approximately 85% of genes
276 altered by maternal stress overlapped with parity-induced gene expression changes. KEGG
277 pathway analysis of DEGs revealed shared enrichment across several pathways in both
278 comparisons, with maternal stress reversing gene expression associated with long-term
279 potentiation, dopaminergic synapses, oxytocin signaling, and other processes (**Fig. 3E**).
280
281 Since our pathway analyses indicated changes in long-term potentiation, a form of neuronal
282 plasticity that is important for learning and memory behaviors[37], we further focused our behavioral
283 assessments on contextual fear conditioning. Consistent with prior results, Control PP females

284 exhibited enhanced acquisition and context recall, as demonstrated by significantly increased
285 freezing behavior compared to NP animals. In contrast, however, Stress PP females showed no
286 significant differences *vs.* NP mice (**Fig. 3F-G**). To further evaluate dHpc-dependent function, we
287 next assessed behavior using the object location task. In this test, animals were initially trained by
288 allowing them to explore two identical objects, followed by one-hour of removal from the arena.
289 During the test phase, one object was displaced, and the animals' ability to identify the moved
290 object was assessed. Given prior findings that adult females require 10 minutes of training for
291 reliable discrimination[38], we first used this duration to confirm that all groups could successfully
292 identify the moved object (**Fig. S3J**). To next assess whether Control PP females exhibit
293 enhancements in this task, we reduced the training time to 5 minutes, a duration that is sufficient
294 for learning in adult males and preadolescent female mice, but not in adult females[38]. Under these
295 conditions, Control PP females retained the ability to discriminate the novel location, whereas NP
296 and Stress PP females did not, reflecting the same pattern observed in contextual fear conditioning,
297 which was not attributed to estrous stage or locomotion (**Fig. S3K-L)**.
298
299 ***Cell-type specific transcriptional alterations reveal dopaminergic modulation underlying***
300 ***maternal dHpc plasticity***
301
302 To elucidate the mechanisms underlying parity-induced dHpc plasticity, we next leveraged the
303 transcriptomic and behavioral signatures shared between NP and Stress PP groups. This
304 postpartum stress paradigm resolves key windows during which disruptions to parity adaptations
305 occur, thereby providing greater temporal resolution of the mechanisms required to sustain these
306 alterations. Building on our findings, we next performed single-nuclei (sn) RNA-sequencing on
307 these three groups to identify the dHpc cell-types that integrate hormone and neurotransmitter
308 signaling to drive parity-related plasticity. Following rigorous quality control assessments to

309 remove confounding sources of variation, such as mitochondrial mapping percentage, doublets,
310 and cell-type contamination **(Fig. S4A-F)**, we retained 109,334 nuclei for downstream analysis
311 (NP = 37,070; Control PP = 35,631; Stress PP = 36,633). Cell-type annotation was performed
312 using both manual curation and label transfer from validated hippocampal datasets from the Broad
313 Institute and Allen Brain Atlas[39,40]. This resulted in 16 distinct clusters (**Fig. 4A, Fig. S4G-I**),
314 including excitatory neuron subtypes (dentate gyrus, CA1, CA3, subiculum, mossy cells; 43.3%
315 of total), GABAergic neurons (GABA.1–GABA.4; 9.1% of total), neural progenitors (neural stem
316 cells, radial glia-like cells; 9.7% of total), and non-neuronal/glial populations (astrocytes,
317 oligodendrocytes, OPCs, microglia, immune cells; 37.9% of total).
318
319 Since our cell-type deconvolution analyses indicated downregulation of neuronal markers, we first
320 assessed proportional differences across major cell-types. A Monte Carlo permutation test
321 confirmed significant shifts in several populations beyond random variation, with GABA.2 and
322 GABA.4 clusters being reduced in Control PP dHpc compared to both NP and Stress PP (**Fig. 4B-**
323 **C**). We next used pseudobulk aggregation and differential expression analysis to identify DEGs
324 within each annotated cluster ($p < 0.05$ and $\log FC > |1.5|$). We observed transcriptional changes
325 across both neuronal and non-neuronal subtypes, with excitatory neuron alterations predominantly
326 observed between NP *vs.* Control PP, particularly within the subiculum (**Fig. 4D**). This pattern
327 aligns nicely with enhanced contextual fear conditioning, as prior studies have implicated altered
328 dHpc excitatory outputs in improved learning outcomes in dams[27]. In contrast, the most
329 pronounced neuronal changes between Control and Stress PP were observed in the GABA.2 and
330 mossy cell populations, alongside widespread DEGs across non-neuronal cell-types (**Fig. 4D**);
331 note that differential expression analysis could not be performed for the GABA.4 cluster due to
332 insufficient sample representation in multiple groups. GO term analysis of DEGs from cell-types

333 displaying proportional differences revealed significant enrichment in pathways associated with
334 responses to endogenous stimuli (GABA.2, GABA.1, GABA.3, OPC), cell proliferation
335 (GABA.2, CA1, immune cells), synaptic function (GABA.3, subiculum), and metabolic processes
336 (Oligo.2, GABA.1) across both comparisons (**Fig. 4E-F**).
337
338 Probing deeper into these altered cell-types, we focused on the GABA.2 cluster owing to shared
339 proportional and transcriptional changes observed in comparison to both NP and Stress PP groups,
340 which suggested a common mechanism limiting dHpc plasticity. Marker gene analysis revealed
341 the significant enrichment of dopamine receptor D1 *(Drd1)* and D2 *(Drd2)* expression within this
342 cluster compared to other cell-types (**Fig. S4J**), aligning with our prior bioinformatic analyses
343 implicating dopaminergic regulation. To further resolve this population, we subclustered the
344 GABA.2 cells and identified distinct subpopulations expressing *Drd1* and *Drd2*, both of which
345 appeared to be altered in Control PP animals (**Fig. 4G**). In a separate cohort of mice, we validated
346 these changes using RNA fluorescence in situ hybridization (FISH) in dorsal CA1 (**Fig. 4H-I, Fig.**
347 **S4K-L**), where dopamine receptor-expressing interneurons have been previously described[41,42].
348 While dopaminoceptive inhibitory neurons were implicated in our data**,** we examined whether
349 such changes extend to other dopamine-sensitive neuronal populations. RNA FISH in the dentate
350 gyrus, which contains excitatory *Drd1* and *Drd2*-expressing neurons (in granule and hilar mossy
351 cells, respectively; **Fig. S7A**), revealed significant group differences, alongside expected regional
352 variations consistent with the sparser distribution of dopamine receptor-expressing neurons in
353 CA1[43] **(Fig. 4H-I, Fig. S4M-N).**
354
355 Since these findings established dopaminergic signaling as a potential key mediator of persistent
356 parity-induced adaptations, this prompted us to examine whether maternal stress disrupts this

357 process within its defined postpartum window. Given prior evidence that acute pup separation
358 elevates dopamine levels in NAc[44,45], we first investigated whether a similar response occurs in
359 dHpc. Brain tissues were collected from 10 dpp dams at baseline, 30-minutes, and 3-hours post-
360 separation, as well as 30-minutes post-reunion (**Fig. 4J).** We observed robust increases in
361 dopamine levels in both NAc and dHpc during separation, with expected regional differences
362 reflecting the strength of innervation to these regions (**Fig. 4K**). Next, we reasoned that this initial
363 pup separation may reflect a normal, adaptive maternal response to unexpected offspring removal.
364 Since acute and chronic stress produce different biological responses and behavioral outcomes,
365 this prompted us to next assess the impact of repeated separation stress on dopamine modulation
366 in these brain regions. Indeed, our data revealed distinct dopaminergic responses following acute
367 *vs.* chronic separations, with repeated stress leading to loss of dopamine increases observed in
368 response to pup separation, as well as elevated baseline dopamine in both dHpc and NAc tissues
369 (**Fig. 4L, Fig. S4O**). Loss of induction following chronic stress may stem from elevated baseline
370 levels, which facilitate engagement of autoreceptors and negative feedback mechanisms[46].
371 Similarly, increased release of dopamine in dHpc tissues were not observed in NP females 30-
372 minutes following separation from a littermate (**Fig. S4P**), though this likely lacks the same
373 salience as pup separation. These findings align well with our snRNA-seq observations, in which
374 the reduced dopamine receptor expression resulting from parity reflects an adaptive process to
375 reduce basal dopamine (supported by our transcriptional data in Figs. 2 and 3 showing
376 downregulation of dopamine processes), thereby enabling robust responsiveness to relevant
377 stimuli. In contrast, elevated receptor expression in NP and Stress PP animals may be a
378 downstream effect of greater basal dopamine tone, thereby dampening the efficiency of stimulus-
379 dependent signaling.

380
381 ***Chemogenetic suppression of dopamine release into dHpc recapitulates key features of***
382 ***persistent parity-induced plasticity***
383
384 Based on these observations, we hypothesized that the maintenance of low basal dopamine tone
385 may drive adaptations of the dopamine-sensitive machinery in dHpc to promote long-term
386 behavioral plasticity. To assess this, we chemogenetically suppressed the dopaminergic VTA
387 projection to dHpc by bilaterally expressing a floxed inhibitory neuronal hM4Di-DREADD fused
388 to mCherry (*vs.* floxed mCherry controls) in the VTA, coupled with retrograde AAVs expressing
389 a tyrosine hydroxylase (TH)-dependent Cre recombinase into the dHpc (**Fig. 5A**). Selection of the
390 VTA was guided by our findings that pup separation stress drives coordinated regulation in the
391 dHpc and NAc, along with its established role as a key upstream modulator of dopaminergic
392 signaling in the maternal NAc[47] (also supported by our data; **Fig. S4Q**). We validated this approach
393 by confirming selective mCherry expression in TH+ neurons of the VTA, as well as reduced *Fos*
394 expression following administration of the selective DREADD agonist deschloroclozapine (DCZ;
395 **Fig. 5B, Fig. S5A-B**.) To minimize injection-related stress in this paradigm, we sought to restrict
396 the window of chronic DCZ administrations. Since maternal stress from 10–20 dpp was sufficient
397 to disrupt parity-induced plasticity, we posited that dHpc dopamine suppression during this period
398 may correspondingly be sufficient to promote neuronal adaptations in virgin NP (NP-mCherry,
399 NP-hM4Di; **Fig. 5C**). As our comparisons aimed to determine if chronic dopamine reduction in
400 virgin females can phenocopy parity-induced adaptations, we administered DCZ to postpartum
401 dams in parallel (PP-mCherry, PP-hM4Di).
402
403 After confirming that our approach effectively suppressed dHpc dopamine (**Fig. 5D**) – and did not
404 induce gross metabolic changes (**Fig. S5C**) – we assessed behavioral outcomes 1-month after the
405 final DCZ injection (49 dpp). In the pup retrieval test, NP-hM4Di females exhibited significantly

406 reduced latency to retrieve pups compared to NP-mCherry, with no differences observed relative
407 to PP dams (**Fig. 5E**). Notably, while 8/13 NP-mCherry females failed to retrieve either pup, this
408 occurred in only 1/15 NP-hM4Di animals, comparable to PP-mCherry (0/12) and PP-hM4di (1/11)
409 dams. In contextual fear conditioning, NP-hM4Di females demonstrated enhanced acquisition,
410 mirroring the heightened learning observed in PP dams (**Fig. 1F**). In the context recall test, NP-
411 hM4Di females showed no significant differences from PP dams (**Fig. S5D**), though subtle effects
412 were observed, suggesting that additional neuromodulatory mechanisms may interact with
413 dopamine to modulate the consolidation and retrieval of conditioned fear responses underlying
414 maternal behavioral plasticity.
415
416 Next, we examined whether such dopamine suppression influences cellular receptor expression in
417 the dHpc. Similar to Control PP, NP-hM4Di females exhibited sustained downregulation of *Drd1*
418 and *Drd2* in both CA1 and dentate gyrus (**Fig. 5G-H, Fig. S5E-H**), thus highlighting the lasting
419 impact of prior dopamine modulation on dHpc receptor dynamics. Finally, we conducted
420 transcriptional profiling of the dHpc in virally infected groups to assess the degree to which
421 dopamine suppression mirrors parity-associated gene expression patterns. Comparing NP-
422 mCherry *vs.* PP-mCherry expression profiles from bulk RNA-seq data, we observed an
423 intermediate expression pattern in NP-hM4Di dHpc tissues (**Fig. 5I, Table S7**). RRHO analysis
424 further supported transcriptional concordance between PP-mCherry and NP-hM4Di groups in
425 comparison to NP-mCherry (**Fig. 5J**). To next assess whether the long-term transcriptional effects
426 of prior baseline dopamine suppression align with changes in parity-associated transcriptional
427 programs, we compared NP-mCherry *vs.* NP-hM4Di DEGs to previously identified parity-
428 sensitive modules. Consistent with our behavioral findings, DEGs from NP-hM4Di overlapped
429 with the brown module but not other parity-sensitive modules (**Fig. 5K**), thereby highlighting a

specific mechanistic contributor to behavioral adaptations within the broader transcriptional and neuromodulatory landscape shaped by parity. Functional annotation of these DEGs revealed enrichment in pathways governing synaptic plasticity and responses to endogenous stimuli (**Fig. 5J**), which mirrored those found to be altered in Control PP dHpc and reinforced dopamine modulation as a key driver of long-lasting maternal brain adaptations (**Fig. S5I**).

DISCUSSION

Despite decades of evidence that matrescence induces long-lasting behavioral adaptations across species, the mechanisms underlying these phenomena remain poorly understood. Through controlled brain-wide, time-course, and cell type-specific transcriptomic analyses – paired with robust behavioral outputs, – we identified gene networks, reproductive events, and neuromodulatory pathways that dynamically shape regional sensitivity across pregnancy and postpartum experiences, thereby promoting plasticity long after these stages have ended. Furthermore, using a maternal-pup separation paradigm during postpartum, we found that modulation of dopamine dynamics is essential for sustaining long-term neural and behavioral adaptations in maternal dHpc. Given dopamine's role in reinforcing maternal behavior and reward, the observed downregulation of dopamine pathways in maternal brain was unexpected, though supported by a prior study[48]. Interestingly, reducing baseline dopamine may enhance the signal-to-noise ratio (SNR) of maternal responses to relevant cues, whereas elevated baseline dopamine levels may impair this process. Indeed, in this study we established the necessity and sufficiency of maintaining appropriate dopamine tone for parity-related dHpc plasticity, demonstrating that chronic dopamine elevation through maternal stress, and chemogenetic suppression within virgin dHpc, bidirectionally modulate parity-related changes at transcriptional, behavioral, and cellular levels. Such findings thus implicate dopamine as a key driver of long-term maternal brain

454 remodeling. These findings expand upon the prevailing view that maternal dopamine function is
455 solely driven by transient surges during maternal behaviors, instead revealing a concurrent
456 downregulation of dopamine tone in critical regions, such as the dHpc, to optimize stimuli
457 sensitivity and behavioral responsiveness.

458

459 ***Ethological significance of maternal dHpc plasticity***

460 Why the dHpc? Improvement of classic dHpc functions, such as spatial cognition, represents
461 evolutionarily advantageous modes for maternal success by enabling more efficient resource
462 foraging and nest navigation[49,50]. Additional dHpc functions, including novelty detection and
463 sensory integration, may also heighten sensitivity to salient environmental cues that are essential
464 for offspring survival[51,52]. Indeed, heightened hippocampal activation in response to one's own
465 infant's cry in human fMRI studies underscores the diverse functional adaptations of this region[53],
466 suggesting a broad range of dHpc modifications that may converge to enhance maternal success.
467 Although chronic maternal stress disrupts the normal trajectory of dHpc adaptations, it remains
468 unclear whether such disruptions are maladaptive or represent evolved coping mechanisms in
469 response to repeated separations. Furthermore, whether stress effects arise from reduced pup
470 interactions, chronic stress exposures, or increased licking, grooming, and/or nursing upon pup
471 reunion is difficult to disentangle within the current model[54]. Notably, unexpected parenting
472 disruptions and resulting adjustments generate significant stress, with parenting-related
473 psychosocial stress uniquely contributing to perinatal and postpartum disorders[55]. Moreover, as
474 pup separation only reduces total pup exposure by ~6.5%, it is unlikely that reduced pup
475 interactions alone account for these effects. Notably, chronic restraint stress during pregnancy
476 similarly disrupts parity-induced spatial memory enhancements[27]. Moreover, human studies show

477 that maternal early life stress alters hippocampal responses to infant cues[56,57], supporting chronic
478 stress as a common interferer in the normal trajectory of maternal dHpc neuroadaptations.

479 Interestingly, we observed natural variation in maternal responses to both acute and chronic stress,
480 as reflected by variability in dHpc transcriptional changes, behavioral outcomes, and dopamine
481 release following pup separation. This suggests that individual differences in maternal motivation
482 or caregiving may influence dopaminergic responses to pup separation, as previously reported[45,58].
483 Interestingly, while the spectrum of outcomes in Stress PP dams indicate variability in stress
484 effects, corticosterone levels were uniformly elevated across all dams following pup separation.
485 This suggests that while chronic stress perturbs parity adaptations, these disruptions are mediated
486 by individual dopamine dynamics downstream of maternal stress responses.

487 ***Dopaminergic regulation of parity adaptations***

488 Our findings, which reveal largescale transcriptional re-programming across the maternal brain,
489 suggest that regions beyond the dHpc also undergo dopamine-mediated adaptations. Indeed, pup
490 separation similarly increases dopamine release in the NAc[44,45], while chronic separations
491 dysregulate this induction by elevating basal dopamine concentrations, thereby facilitating
492 engagement of negative feedback mechanisms[46]. Importantly, this perturbation offers insight into
493 normal maternal dopamine regulation, emphasizing the need for low postpartum dopamine tone to
494 enable signaling induction to relevant stimuli[27,59]. Moreover, as restraint stress enhances
495 dopaminergic burst firing, and chronic gestational restraint impairs spatial learning, we propose
496 that dopamine dysregulation serves as a common mode of dysregulating parity-related
497 neuroadaptations across reproductive stages.

498 How do postpartum alterations drive sustained behavioral changes? Our findings reveal that
499 downregulation of dopamine transcriptional networks in Control PP dHpc corresponds with
500 reduced *Drd1/Drd2* expression, whereas elevated baseline dopamine in Stress PP associates with
501 increased receptor expression, likely reflecting compensations to tonic dopamine dynamics during
502 matrescence and/or chronic stress, rather than loss of dopaminoceptive cells. Notably, receptor
503 downregulation may also contribute to structural plasticity, as parity is linked to dendritic
504 remodeling in CA1 and CA3[7], paralleling gray matter reductions observed in mothers years after
505 parturition[1,2,4,22]. Thus, our work points to two mechanisms potentially underlying maternal dHpc
506 adaptations: alterations in *Drd1/Drd2* receptor expression and shifts in baseline dopamine tone.
507
508 Given that *Drd1/Drd2*-expressing GABAergic neurons contribute to both aversive contextual
509 memory formation and maternal behavior[45,60–64], receptor expression changes likely intersect with
510 these functions. Alternatively, receptor shifts may not directly influence behavior but instead
511 reflect downstream consequences of altered dopamine tone. Within this framework, maintenance
512 of low dopamine tone in Control PP dHpc may serve to reduce background noise, enhancing the
513 processing of relevant cues by increasing SNR[65]. In addition to limiting negative feedback, low
514 dopamine tone also prolongs and amplifies phasic dopamine responses to stimuli[66]. As phasic
515 dopamine responses are essential for memory formation[67,68], this process may underlie parity-
516 induced enhancements in fear conditioning outcomes. While not traditionally considered a
517 maternal behavior-regulating region, the dHpc integrates sensory, novelty, and salience
518 information to shape pup retrieval responses. Consistent with our findings, lesion studies
519 corroborate hippocampal involvement in pup retrieval behavior[69,70]. Moreover, hippocampal
520 activity modulates downstream circuits via the polysynaptic VTA-hippocampal loop, which
521 projects to the NAc and ventral pallidum - key regulators of pup retrieval[52,63]. Enhanced SNR

522 within the dHpc may thus enable more efficient processing of offspring cues, facilitating robust
523 behavioral responses to both rewarding and aversive stimuli through signal processing across this
524 broader network.
525
526 These findings expand upon a broader maternal neuroadaptive process in which enhanced SNR
527 optimizes responsiveness to offspring-related stimuli. Similar mechanisms have been described
528 for oxytocin signaling, which enhances sensory salience by increasing SNR across multiple brain
529 regions[71]. For example, in the left auditory cortex, oxytocin disinhibits pyramidal neuron activation
530 in response to pup calls, enabling pup retrieval behaviors in previously non-maternal virgins[72]. In
531 humans, disinhibition of cognitive and affective regions has also been associated with more
532 responsiveness in maternal brains[73]. Similarly, estradiol and progesterone modulate SNR by
533 reducing baseline activity of galanin-expressing mPOA neurons, leading to a reduced
534 depolarization block that enhances responsiveness to pup stimuli[18]. Although these effects occur
535 acutely in response to pregnancy hormones, they persist beyond postpartum[18], mirroring the long-
536 term neural adaptations observed in our study.

537 ***Broader implications of maternal brain remodeling***

538 While our study focused largely on dopamine, it is notable that our chemogenetic manipulations
539 recapitulated key transcriptional and behavioral outcomes of parity, albeit not to the same extent.
540 This underscores dopamine as a crucial but not exclusive driver of parity-induced adaptations.
541 Indeed, our data also implicate hormonal contributions, including estrogen, progesterone, and
542 oxytocin signaling, in shaping transcriptional programming. Consistent with this, previous studies
543 have linked parity to estradiol-driven neuronal alterations[12], while others have demonstrated that
544 blocking oxytocin signaling disrupts parity-induced spatial learning enhancements[30]. These

545 findings suggest that parity programming arises from integration of multiple neuromodulatory
546 pathways to induce long-term effects. However, given that estrogen signaling during postpartum
547 regulates oxytocin release, which in turn modulates VTA signaling, we propose that dopamine
548 adaptations serve as a key downstream mechanism within a broader network driving sustained
549 maternal neuroplasticity[74].

550 What upstream mechanisms may regulate dopamine adaptations in maternal brain? As discussed,
551 oxytocin regulates VTA dopamine release, yet whether it contributes to enduring changes in VTA-
552 dHpc tone remains unknown. Additionally, the mechanisms by which chronic maternal stress
553 alters this dopaminergic tone warrant further investigation. While this study focused on the VTA
554 as an upstream provider of dHpc dopamine, the LC also provides substantial dopaminergic input
555 to the dHpc, suggesting broader brain region involvement in dopamine-mediated adaptations[68,75].
556 Given its additional involvement in stress signaling, the LC, alongside the VTA, may contribute
557 to signaling processes underlying chronic maternal stress effects. Furthermore, other brain regions,
558 such as hypothalamic inputs, may modulate dHpc dopamine tone in response to stress, representing
559 important avenues for future investigation.

560 Together, this work demonstrates that transient neuromodulatory processes during pregnancy and
561 postpartum drive lasting maternal neuroplasticity. Importantly, this fundamental shift in brain state
562 may interact with future experience-dependent plasticity. As parity is implicated in both risk and
563 resilience to brain disorders[15], future research should account for parity status as a key variable
564 shaping differential outcomes, particularly in its interactions with other risk factors. In particular,
565 our findings highlight an interplay between parity and stress, a key risk factor for brain disorder
566 vulnerability, in shaping maternal brain outcomes. Thus, this study provides novel insights into

567 the gene networks, dynamics, and neuromodulatory pathways that drive long-lasting parity-
568 induced adaptations, while underscoring the importance of stress mitigation during pregnancy and
569 postpartum.

570 **ACKNOWLEDGEMENTS**

571 We would like to thank members of the Maze lab for their helpful discussion on this study, and
572 members of the Nestler, Russo, and Kenny labs at the Icahn School of Medicine at Mount Sinai
573 for providing materials and/or access to behavioral equipment. We thank Dr. Min Chen, Winnie
574 Chen, Emma Andraka, and Rasika Iyer for experimental assistance. This work was partially
575 supported by grants from the National Institutes of Health: R01 MH116900 (I.M.), F32 MH126534
576 (J.C.C.), F31 NS132558 (A.M.C.), F99 NS139541 (A.M.C.), as well as funds from the Brain and
577 Behavior Research Foundation (J.C.C.), and the Howard Hughes Medical Institute (I.M.). All
578 schematics were created with Biorender.com.

579 **DECLARATION OF INTEREST**
580
581 The authors declare no competing interests.
582
583
584 **AUTHOR CONTRIBUTIONS**
585
586 J.C.C. and I.M. conceived of the study, designed the experiments, and interpreted the data. J.C.C.,
587 G.D.S., A.M.C., and S.D. performed behavioral experiments. J.C.C., G.D.S., A.M.C., and S.D.
588 performed surgeries. J.C.C., G.D.S., and C.Z. performed estrous cycle analyses. J.C.C., G.D.S.,
589 and S.D. conducted immunofluorescence and RNAscope analyses. J.C.C. and G.D.S. performed
590 molecular experiments. J.C.C. and E.A.B. performed single-cell sequencing experiments. J.C.C.,
591 G.D.S., and E.W. performed bioinformatic analyses. J.C.C. and I.M. wrote the manuscript.
592

INCLUSION & ETHICS STATEMENT

All collaborators associated with this work have fulfilled the criteria for authorship required by Cell Press journals. To obtain authorship, their participation in this study was deemed to be essential for the design and implementation of the work presented. Roles and responsibilities were agreed upon among collaborators ahead or during the research.

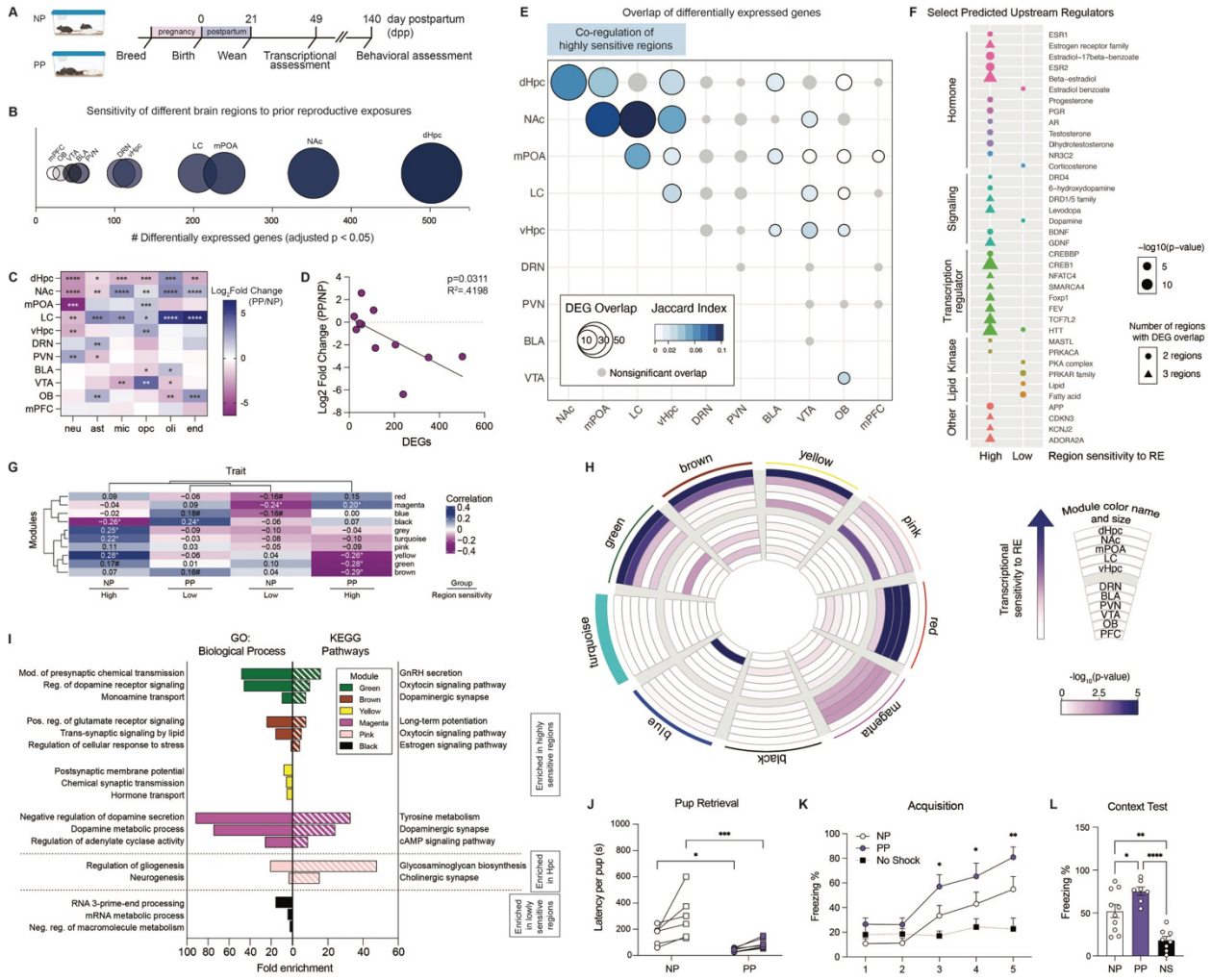

Figure 1. Pregnancy and postpartum states promote lasting transcriptional and behavioral adaptations in the maternal brain. A) Experimental timeline comparing primiparous (PP) *vs.* age-matched nulliparous (NP) female mice 1-month after offspring weaning (day postpartum, 49 dpp), and behavioral outcomes at 140 dpp. **B)** Differentially expressed genes (DEGs) per brain region. Bubble size represents total number of NP *vs.* PP DEGs (adj. $p < 0.05$). **C)** Cell-type deconvolution of bulk RNA-seq data (NP *vs.* PP normalized surrogate proportion variables, Student's t-test with multiple comparisons correction; *FDR < 0.05, **FDR < 0.01, ***FDR < 0.001, ****FDR < 0.0001). **D)** Downregulation of neuron proportion significantly correlated with number of DEGs per brain region ($R^2 = 0.4198$, $p = 0.0311$). **E)** Overlap of DEGs across brain regions ($p < 0.05$; gray indicates nonsignificant overlap). **F)** Select predicted upstream regulators of overlapping DEGs across regions with high (dHpc, NAc, mPOA, LC, vHpc) *vs.* low (DRN, PVN, BLA, VTA, OB, mPFC) sensitivity to parity. **G)** Trait heatmap correlating gene co-expression modules (arbitrary color names, identified by weighted gene correlation network analysis) with group x brain region classification (*p < 0.05, #p < 0.1). **H)** Circos plot for gene co-expression modules, with the size and arbitrary color name of each module indicated by the arc thickness along the perimeter. Enrichment for DEGs per brain region for each module is indicated by the inner rings, with color indicating significance of overlap. **I)** Select GO Biological Processes

and KEGG Pathways significantly enriched from gene co-expression modules (FDR < 0.05). **J)** PP dams retrieved both pups significantly faster compared to NP females at 140 dpp (two-way rmANOVA, main effect of group ($F(1,11) = 14.47$, $p = 0.0029$), main effect of pup number ($F(1,11) = 11.36$, $p = 0.0062$)), with significantly reduced latency for retrieval of pup 1 (Holm-Šídák's multiple comparisons test, $t(22) = 2.301$, *adj. $p = 0.0312$) and pup 2 (Holm-Šídák's multiple comparisons test, $t(22) = 4.098$, ***adj. $p = 0.0009$). N = 6-7 animals/group. **K)** PP dams exhibited increased freezing behavior during the acquisition phase of contextual fear conditioning (two-way rmANOVA, main effect of group ($F(2,21) = 4.259$, $p = 0.028$), main effect of preshock ($F(2.827, 59.36) = 26.59$, $p < 0.0001$), interaction ($F(8,84) = 5.091$, $p < 0.0001$)), compared to no shock controls (Dunnett's multiple comparisons test, *$p \leq 0.05$, **$p < 0.01$). **L)** During the context recall test, PP dams froze significantly more compared to NP (one-way ANOVA, $F(2,22) = 18.72$, $p < 0.0001$; Tukey's multiple comparisons test, $t(22) = 3.640$, *$p = 0.044$), with both groups demonstrating contextual learning compared to no shock controls (PP vs. NS, $t(22) = 8.541$, ****$p < 0.0001$; NP vs. NS, $t(22) = 5.538$, **$p = 0.0021$). N = 7-10 animals/group. Error bars represent mean ± SEM.

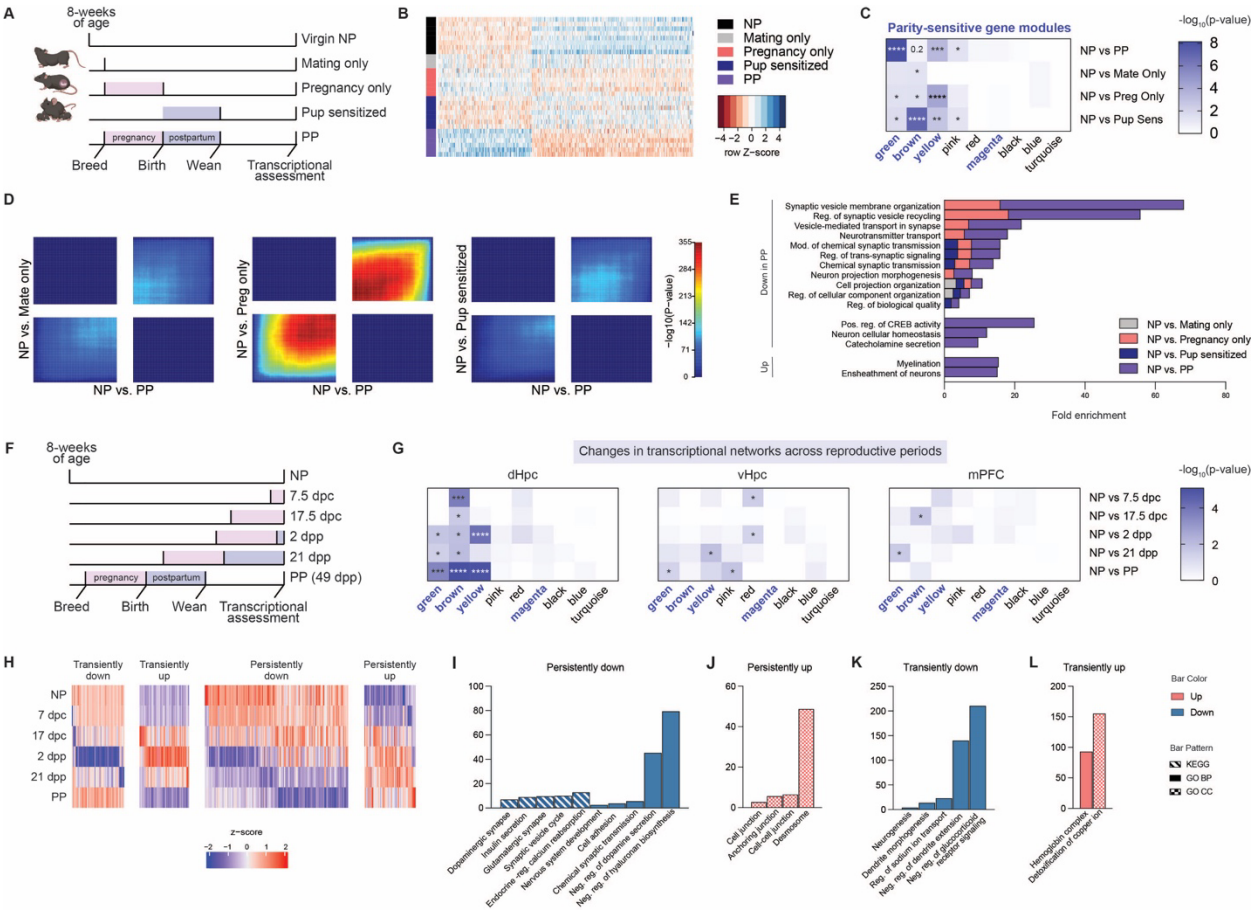

Figure 2. Parity adaptations in the dHpc transcriptome integrate pregnancy and postpartum experiences. A) Experimental design to examine the contribution of discrete female reproductive events. **B)** Heatmap of differential expression profiles of top 500 genes, by ascending p-values, between NP *vs.* PP (N=3-7/group). **C)** Overlap of DEGs (*vs.* NP, adj. $p < 0.05$) for each gene co-expression module, with color representing extent of significance (*$p < 0.05$, **$p < 0.01$, ***$p < 0.001$, ****$p < 0.0001$). High parity sensitivity modules are indicated in bold. **D)** Threshold-free comparison of indicated comparisons by rank-rank hypergeometric overlap. Pixels represent the overlap of differential expression profiles indicated, with color representing extent of significance. The lower left and upper right quadrants represent concordant gene regulation. **E)** Shared changes in biological processes (identified through GO term analysis) observed following individual reproductive exposures with PP, along with processes exclusive to the combined experiences in PP (FDR < 0.05). **F)** Experimental design to examine the trajectory of PP dHpc gene expression changes across pregnancy and postpartum periods (dpc: days post-conception; dpp: days postpartum). **G)** Enrichment of DEGs (*vs.* NP, adj. $p < 0.05$) with parity-sensitive gene co-expression modules across reproductive time points, examining extent of significant overlap in brain regions exhibiting high (left, dHpc), moderate (middle, vHpc), and low (right, mPFC) transcriptional sensitivity to parity status (*$p < 0.05$, **$p < 0.01$, ***$p < 0.001$, ****$p < 0.0001$). N=6/group. **H)** Impulse time course analysis of dHpc gene expression identified patterns of transient *vs.* persistent up- and downregulation across pregnancy and postpartum (FDR < 0.05). **I-L)** Select GO terms and KEGG pathways significantly enriched for dHpc genes exhibiting patterns

658 of **(I)** persistent downregulation, **(J)** persistent upregulation, **(K)** transient downregulation, and **(L)**
659 transient upregulation across reproductive stages (FDR < 0.05).
660

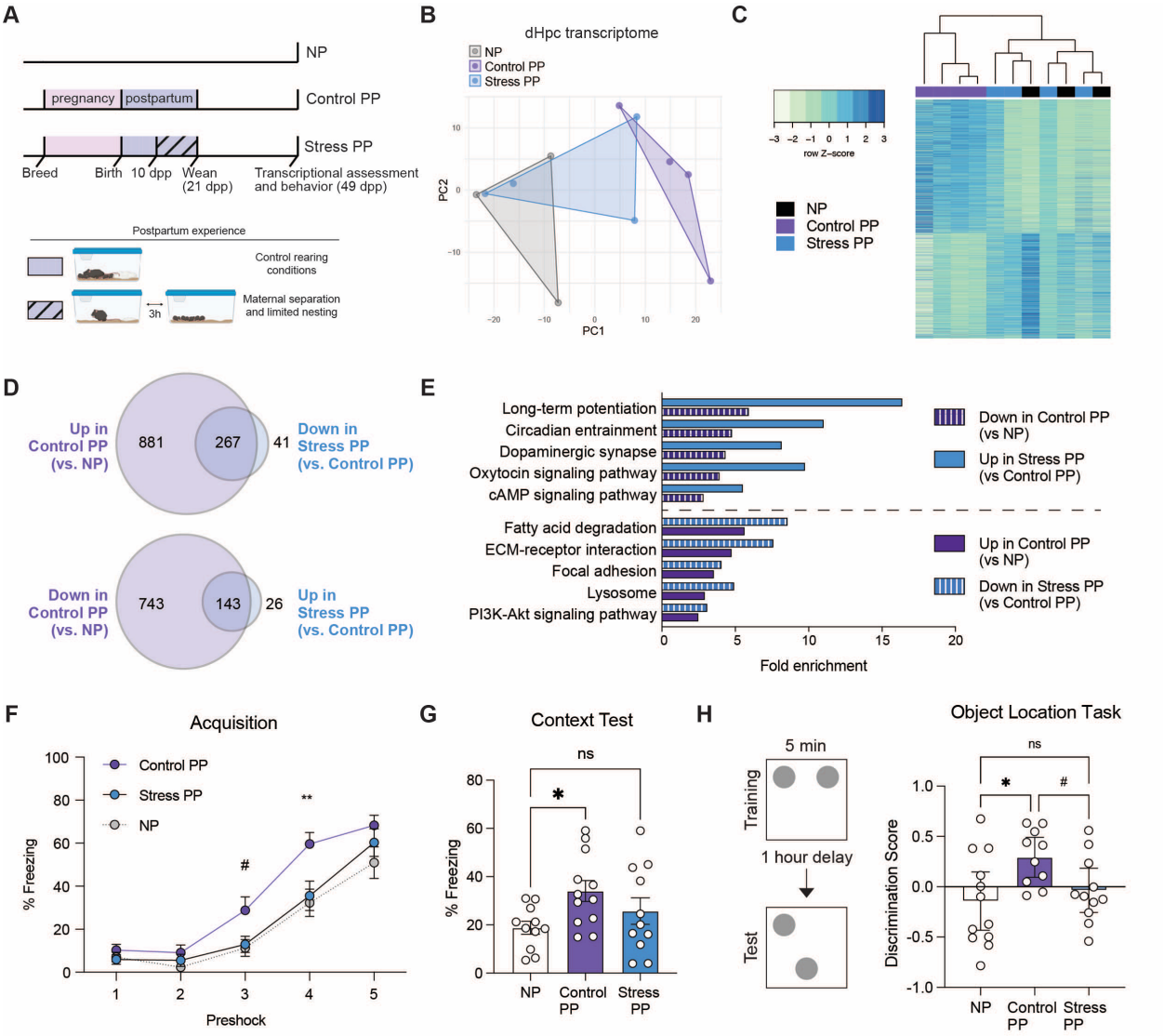

Figure 3. Postpartum stress disrupts long-term maternal dHpc adaptations. A) Postpartum stress paradigm, wherein dams were provided with limited nesting and subjected to pup separation 3 hours daily between 10-20 dpp, followed by behavioral and transcriptomic assessments at 49 dpp. **B)** Principal components analysis of dHpc transcriptomes, and **C)** heatmap of all significant DEGs (adj. $p < 0.05$) with hierarchical clustering. **D)** Venn Diagrams showing ~20% DEGs altered in Control PP (*vs.* NP) are significantly disrupted by postpartum stress (adj. $p < 0.05$). **E)** Parity-dependent enrichment in select KEGG pathways are significantly reversed in Stress PP (FDR < 0.05). **F)** Control PP dams froze more during the acquisition phase of contextual fear conditioning (two-way rmANOVA, main effect of group ($F(2,31) = 4.662$, $p = 0.017$), main effect of preshock ($F(3.024,93.75) = 129.8$, $p < 0.0001$), interaction ($F(8,124) = 2.406$, $p = 0.091$)), compared to NP and Stress PP (Tukey's multiple comparisons test, #$p \leq 0.1$, *$p < 0.05$, **$p < 0.01$). **G)** During the context recall test, NP froze significantly less than Control PP (one-way ANOVA, $F(2,31) = 3.151$, $p = 0.05$; Tukey's multiple comparisons test, $t(31) = 3.54$, *$p = 0.0456$), but not Stress PP (ns, $p > 0.05$). N = 11-12 animals/group. **H)** Control PP, but not Stress PP, dams spent more time investigating the moved object in the object location task compared to NP (one way ANOVA,

$F(2,30) = 4.045$, $p = 2.0278$; Holm-Šídák's multiple comparisons test: NP vs. Control PP, $t(30) = 2.764$, *adj. $p = 0.0288$; Control PP vs. Stress PP, $t(30) = 2.046$, #adj. $p < 0.1$) N=10-12 animals/group. Error bars represent mean ± SEM.

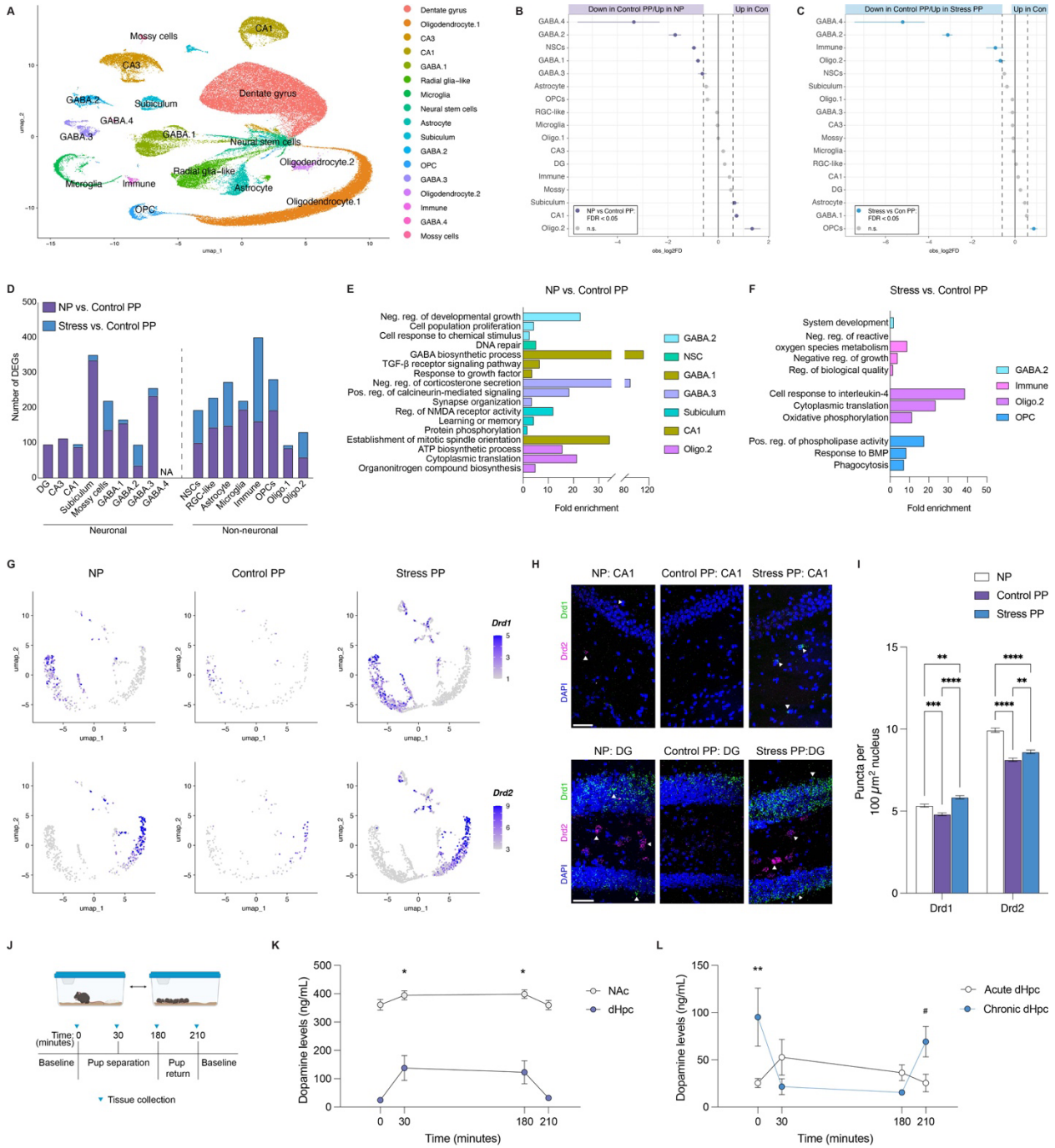

Figure 4. Parity-driven dHpc plasticity is suppressed by elevated dopamine signaling. A) UMAP representation of cell clusters (109,334 total cells) from dHpc tissues, colored by major cell types (N = 6 NP, 4 Control PP, 5 Stress PP). **B, C)** Point range plots depicting significant changes in proportions of major cell-type clusters between **(B)** NP vs. Control PP, and **(C)** Stress PP vs. Control PP (FDR < 0.05 and $|\log_2\text{Differerence}| > \log_2(1.5)$). **D)** Number of DEGs observed for each major cell-type following pseudobulk analysis ($p < 0.05$ and $|\log_2(\text{Fold Change})| > \log_2(1.5)$). **E, F)** GO term analyses (Biological Process) for DEGs identified in cell clusters with

692 significant proportional differences between **(E)** NP vs. Control PP, and **(F)** Stress vs. Control PP
693 (FDR < 0.05). **G)** Subclustering of GABA.2 neuronal population revealed reductions in *Drd1* (top)
694 and *Drd2* (bottom) expression in Control PP. **H)** Representative images of RNAScope for *Drd1*
695 and *Drd2* mRNAs in dorsal CA1 (top) and dentate gyrus (DG, bottom). Scale bars, 50 µm. **I)**
696 Quantification of *Drd1* and *Drd2* mRNA puncta in CA1 and DG nuclei (two-way ANOVA, main
697 effect of group ($F(2,82142) = 65.81$, $p < 0.0001$), main effect of gene ($F(1,82142) = 1771$, $p <$
698 0.0001), interaction ($F(2,82142) = 39.99$, $p < 0.0001$); Tukey's multiple comparisons test, **p <
699 0.01, ***p < 0.001, ****p < 0.0001). N = 5 animals/group. **J)** Experimental design of pup
700 separation test to examine changes in brain tissue dopamine levels. **K)** Pup separation significantly
701 increases dopamine levels from baseline in dHpc and NAc tissues (two-way ANOVA, main effect
702 of time ($F(3,52) = 4.287$, $p = 0.0089$), main effect of brain region ($F(1,52) = 225.7$, $p < 0.0001$;
703 interaction ($F3,52) = 1.086$, $p = 0.3717$), with significant increases in dHpc dopamine levels
704 (Dunnett's multiple comparisons test, *p < 0.05, **p < 0.01). N = 5-9 animals/time point. **L)**
705 Chronic pup separations increases baseline dHpc dopamine concentrations (two-way ANOVA,
706 interaction ($F(3,53) = 4.822$, $p = 0.0048$; group $(1, 53) = 1.876$), $p = 0.1708$, time $(3, 53) = 1.736$,
707 $p = 0.1706$; Tukey's multiple comparisons test, *p < 0.05, #p = 0.06). N = 5-12 animals/time point.
708 Error bars represent mean ± SEM.
709

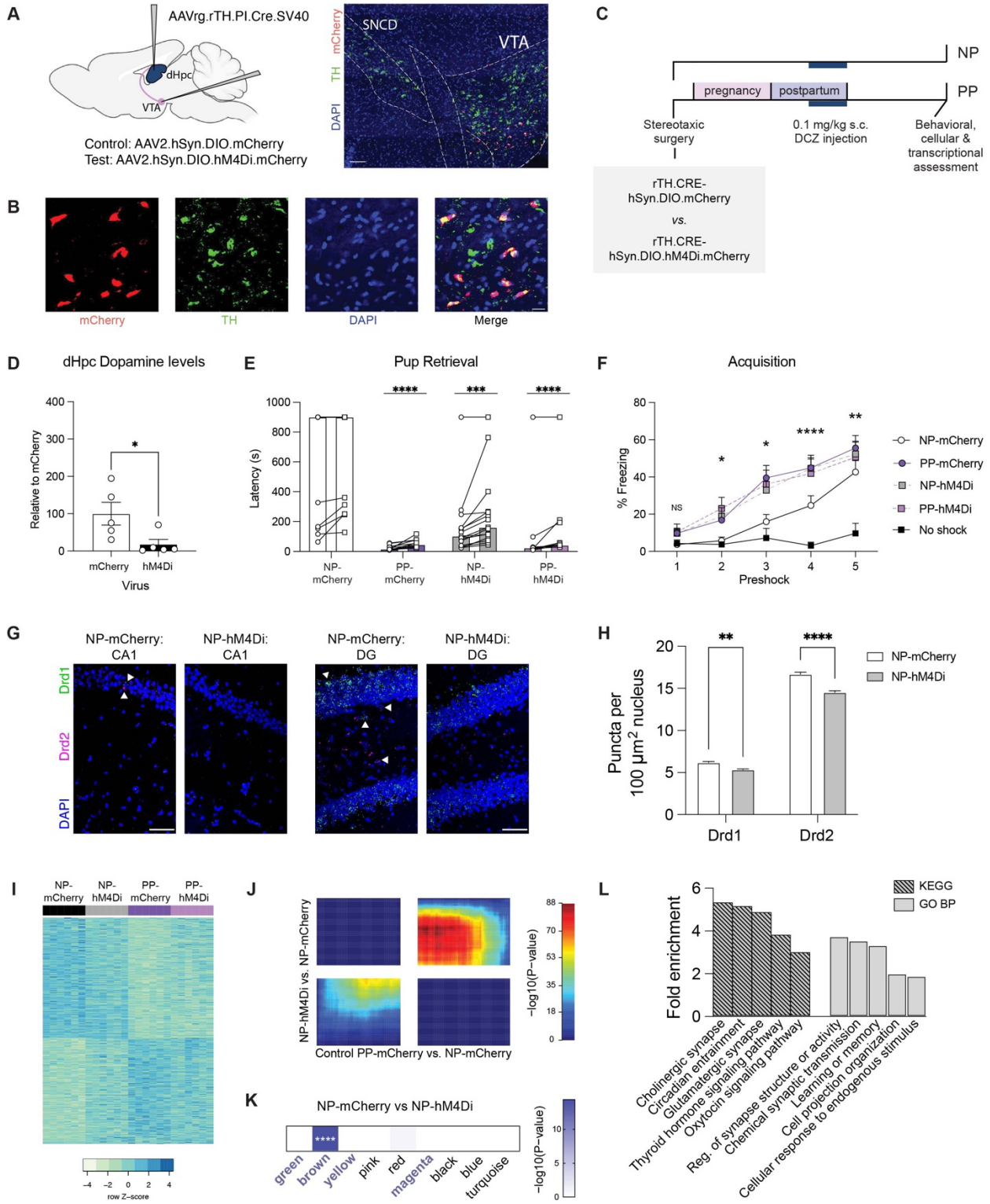

Figure 5. Chronic dopamine suppression is sufficient to phenocopy persistent maternal dHpc plasticity. A) Experimental design (left) and representative image (right) of AAV2.hSyn.DIO.mCherry targeting to VTA projection neurons following dHpc injection of

716 retrograde (rg) Cre under control of the tyrosine hydroxylase (TH) promoter. Scale bar, 100 µm.
717 **B)** Representative images showing overlap of virally-induced mCherry with TH+ cells in VTA.
718 Scale bar, 20 µm. **C)** Timeline of stereotaxic surgeries and s.c. deschloroclozapine (DCZ)
719 injections from 10-20 dpp in NP and PP female mice, followed by experimental assessments
720 starting at 49 dpp. **D)** Significant reduction in dHpc dopamine levels following inhibition of VTA
721 projection neurons (Student's t-test:$t(8) = 2.477$, $*p = 0.0383$). N=5/group. **E)** PP-mCherry, NP-
722 hM4Di, and PP-hM4Di retrieved pups faster than NP-mCherry (two-way rmANOVA, main effect
723 of group ($F(3,47) = 14.39$, $p < 0.0001$), main effect of pup number ($F(1, 47) = 18.96$, $p < 0.0001$;
724 Sidak's multiple comparisons test, $****p < 0.0001$, $***p < 0.001$). N =11-15/group. Bar
725 represents mean. **F)** PP-mCherry, NP-hM4Di, and PP-hM4Di freeze more compared to no shock
726 controls at earlier phases of contextual fear acquisition, compared to NP-mCherry (two-way
727 rmANOVA, main effect of group ($F(4,41) = 4.739$, $p = 0.0031$), main effect of preshock
728 ($F(2.818,115.5) = 61.92$, $p < 0.0001$), interaction ($F(16,164) = 2.606$, $p = 0.0012$; Tukey's multiple
729 comparisons test, $*p \leq 0.05$, $**p < 0.01$, $****p < 0.0001$). N = 9-12/group. Error bars represent
730 mean ± SEM. **G)** Representative images of RNAScope for *Drd1* and *Drd2* mRNAs in dorsal CA1
731 (top) and DG (bottom). Scale bars, 50 µm. **H)** Quantification of *Drd1* and *Drd2* mRNA puncta in
732 CA1 and DG nuclei (two-way ANOVA, main effect of group ($F(2,33404) = 64.43$, $p < 0.0001$),
733 main effect of gene ($F(1,33404) = 2770$, $p < 0.0001$), interaction ($F(2,33404) = 12.52$, $p = 0.0004$);
734 Sidak's multiple comparisons test, $**p < 0.01$, $****p < 0.0001$). N = 3 animals/group. **I)** Bulk
735 dHpc differential expression profiles of top 500 genes (by ascending p-values) between NP-
736 mCherry and PP-mCherry. N=6/group. **J)** Threshold-free comparison by rank-rank
737 hypergeometric overlap, showing concordant gene regulation (bottom left and upper right
738 quadrants) between the comparisons indicated. **K)** Overlap of DEGs (NP-hM4Di vs. NP-mCherry,
739 adj. $p < 0.05$) with gene co-expression modules ($****p < 0.0001$). High parity sensitivity modules
740 are indicated in bold. **L)** Select GO terms and KEGG pathways significantly enriched for NP-
741 mCherry vs. NP-hM4Di DEGs (FDR < 0.05).
742

SUPPLEMENTARY MATERIALS

Materials and Methods
Figs. S1 to S5
Tables S1 to S7
Supplemental References

REFERENCES

1. Hoekzema, E. *et al.* Pregnancy leads to long-lasting changes in human brain structure. *Nature neuroscience* **20**, 287–296 (2017).
2. Martínez-García, M. *et al.* Do Pregnancy-Induced Brain Changes Reverse? The Brain of a Mother Six Years after Parturition. *Brain sciences* **11**, 168 (2021).
3. Voldsbekk, I. *et al.* A history of previous childbirths is linked to women's white matter brain age in midlife and older age. *Human Brain Mapping* **42**, 4372–4386 (2021).
4. Pritschet, L. *et al.* Neuroanatomical changes observed over the course of a human pregnancy. *Nat Neurosci* 1–8 (2024) doi:10.1038/s41593-024-01741-0.
5. de Lange, A.-M. G. *et al.* Population-based neuroimaging reveals traces of childbirth in the maternal brain. *Proceedings of the National Academy of Sciences* **116**, 22341 LP – 22346 (2019).
6. de Lange, A.-M. G. *et al.* The maternal brain: Region-specific patterns of brain aging are traceable decades after childbirth. *Human Brain Mapping* **41**, 4718–4729 (2020).
7. Pawluski, J. L. & Galea, L. A. M. Hippocampal morphology is differentially affected by reproductive experience in the mother. *Journal of neurobiology* **66**, 71–81 (2006).
8. Duarte-Guterman, P. *et al.* Cellular and molecular signatures of motherhood in the adult and ageing rat brain. *Open Biology* **13**, 230217 (2023).
9. Workman, J. L. *et al.* Parity modifies the effects of fluoxetine and corticosterone on behavior, stress reactivity, and hippocampal neurogenesis. *Neuropharmacology* **105**, 443–453 (2016).
10. Macbeth, A. H., Scharfman, H. E., Maclusky, N. J., Gautreaux, C. & Luine, V. N. Effects of multiparity on recognition memory, monoaminergic neurotransmitters, and brain-derived neurotrophic factor (BDNF). *Hormones and behavior* **54**, 7–17 (2008).
11. Kinsley, C. H. & Lambert, K. G. Reproduction-Induced Neuroplasticity: Natural Behavioural and Neuronal Alterations Associated with the Production and Care of Offspring. *Journal of Neuroendocrinology* **20**, 515–525 (2008).
12. Barha, C. K., Lieblich, S. E., Chow, C. & Galea, L. A. M. Multiparity-induced enhancement of hippocampal neurogenesis and spatial memory depends on ovarian hormone status in middle age. *Neurobiology of Aging* **36**, 2391–2405 (2015).
13. Meurisse, M. *et al.* Estradiol receptor-α expression in hypothalamic and limbic regions of ewes is influenced by physiological state and maternal experience. *Hormones and Behavior* **48**, 34–43 (2005).
14. Love, G. *et al.* Maternal Experience Produces Long-Lasting Behavioral Modifications in the Rat. *Behavioral Neuroscience* **119**, 1084–1096 (2005).
15. Deems, N. P. & Leuner, B. Pregnancy, postpartum and parity: Resilience and vulnerability in brain health and disease. *Frontiers in Neuroendocrinology* **57**, 100820 (2020).
16. Figueiredo, B. & Conde, A. Anxiety and depression symptoms in women and men from early pregnancy to 3-months postpartum: Parity differences and effects. *Journal of Affective Disorders* **132**, 146–157 (2011).
17. Martínez-Galiano, J. M., Hernández-Martínez, A., Rodríguez-Almagro, J., Delgado-Rodríguez, M. & Gómez-Salgado, J. Relationship between parity and the problems that appear in the postpartum period. *Sci Rep* **9**, 11763 (2019).
18. Ammari, R. *et al.* Hormone-mediated neural remodeling orchestrates parenting onset during pregnancy. *Science* **382**, 76–81 (2023).

19. Leuner, B., Glasper, E. R. & Gould, E. Parenting and plasticity. *Trends in Neurosciences* **33**, 465–473 (2010).
20. Bridges, R. S. Neuroendocrine Regulation of Maternal Behavior. *Front Neuroendocrinol* **0**, 178–196 (2015).
21. McKenzie, A. T. *et al.* Brain Cell Type Specific Gene Expression and Co-expression Network Architectures. *Scientific Reports* **8**, 8868 (2018).
22. Paternina-Die, M. *et al.* Women's neuroplasticity during gestation, childbirth and postpartum. *Nat Neurosci* **27**, 319–327 (2024).
23. Langfelder, P. & Horvath, S. WGCNA: an R package for weighted correlation network analysis. *BMC Bioinformatics* **9**, 559 (2008).
24. Bridges, R. S. Long-term effects of pregnancy and parturition upon maternal responsiveness in the rat. *Physiology & Behavior* **14**, 245–249 (1975).
25. Pawluski, J. L., Vanderbyl, B. L., Ragan, K. & Galea, L. A. M. First reproductive experience persistently affects spatial reference and working memory in the mother and these effects are not due to pregnancy or 'mothering' alone. *Behavioural Brain Research* **175**, 157–165 (2006).
26. Pawluski, J. L., Walker, S. K. & Galea, L. A. M. Reproductive experience differentially affects spatial reference and working memory performance in the mother. *Horm Behav* **49**, 143–149 (2006).
27. Lemaire, V. *et al.* Motherhood-induced memory improvement persists across lifespan in rats but is abolished by a gestational stress. *The European journal of neuroscience* **23**, 3368–3374 (2006).
28. Gatewood, J. D. *et al.* Motherhood mitigates aging-related decrements in learning and memory and positively affects brain aging in the rat. *Brain research bulletin* **66**, 91–98 (2005).
29. Macbeth, A. H., Gautreaux, C. & Luine, V. N. Pregnant rats show enhanced spatial memory, decreased anxiety, and altered levels of monoaminergic neurotransmitters. *Brain research* **1241**, 136–147 (2008).
30. Tomizawa, K. *et al.* Oxytocin improves long-lasting spatial memory during motherhood through MAP kinase cascade. *Nature Neuroscience* **6**, 384–390 (2003).
31. Paris, J. J. & Frye, C. A. Estrous cycle, pregnancy, and parity enhance performance of rats in object recognition or object placement tasks. *Reproduction* **136**, 105–115 (2008).
32. Stolzenberg, D. S. & Rissman, E. F. Oestrogen-independent, experience-induced maternal behaviour in female mice. *J Neuroendocrinol* **23**, 345–354 (2011).
33. Cahill, K. M., Huo, Z., Tseng, G. C., Logan, R. W. & Seney, M. L. Improved identification of concordant and discordant gene expression signatures using an updated rank-rank hypergeometric overlap approach. *Scientific Reports* **8**, 9588 (2018).
34. Fischer, D. S., Theis, F. J. & Yosef, N. Impulse model-based differential expression analysis of time course sequencing data. *Nucleic Acids Research* **46**, e119 (2018).
35. McArdle, H. J. The metabolism of copper during pregnancy —a review. *Food Chemistry* **54**, 79–84 (1995).
36. Leuner, B. & Sabihi, S. The birth of new neurons in the maternal brain: Hormonal regulation and functional implications. *Frontiers in neuroendocrinology* **41**, 99–113 (2016).
37. Lynch, M. A. Long-Term Potentiation and Memory. *Physiological Reviews* **84**, 87–136 (2004).

842 38. Le, A. A. *et al.* Prepubescent female rodents have enhanced hippocampal LTP and learning
843 relative to males, reversing in adulthood as inhibition increases. *Nat Neurosci* **25**, 180–190
844 (2022).
845 39. Habib, N. *et al.* Div-Seq: Single-nucleus RNA-Seq reveals dynamics of rare adult newborn
846 neurons. *Science* **353**, 925–928 (2016).
847 40. Yao, Z. *et al.* A taxonomy of transcriptomic cell types across the isocortex and hippocampal
848 formation. *Cell* **184**, 3222-3241.e26 (2021).
849 41. Gangarossa, G. *et al.* Characterization of dopamine D1 and D2 receptor-expressing neurons
850 in the mouse hippocampus. *Hippocampus* **22**, 2199–2207 (2012).
851 42. Puighermanal, E. *et al.* Anatomical and molecular characterization of dopamine D1
852 receptor-expressing neurons of the mouse CA1 dorsal hippocampus. *Brain Struct Funct*
853 **222**, 1897–1911 (2017).
854 43. Godino, A. *et al.* Dopaminoceptive D1 and D2 neurons in ventral hippocampus arbitrate
855 approach and avoidance in anxiety. 2023.07.25.550554 Preprint at
856 https://doi.org/10.1101/2023.07.25.550554 (2023).
857 44. Hansen, S., Bergvall, Å. H. & Nyiredi, S. Interaction with pups enhances dopamine release
858 in the ventral striatum of maternal rats: A microdialysis study. *Pharmacology Biochemistry*
859 *and Behavior* **45**, 673–676 (1993).
860 45. Champagne, F. A. *et al.* Variations in nucleus accumbens dopamine associated with
861 individual differences in maternal behavior in the rat. *J Neurosci* **24**, 4113–4123 (2004).
862 46. Ford, C. P. The Role of D2-Autoreceptors in Regulating Dopamine Neuron Activity and
863 Transmission. *Neuroscience* **282**, 13–22 (2014).
864 47. Shahrokh, D. K., Zhang, T.-Y., Diorio, J., Gratton, A. & Meaney, M. J. Oxytocin-
865 Dopamine Interactions Mediate Variations in Maternal Behavior in the Rat. *Endocrinology*
866 **151**, 2276–2286 (2010).
867 48. Afonso, V. M., Grella, S. L., Chatterjee, D. & Fleming, A. S. Previous maternal experience
868 affects accumbal dopaminergic responses to pup-stimuli. *Brain Research* **1198**, 115–123
869 (2008).
870 49. Pawluski, J. L., Lambert, K. G. & Kinsley, C. H. Neuroplasticity in the maternal
871 hippocampus: Relation to cognition and effects of repeated stress. *Hormones and Behavior*
872 **77**, 86–97 (2016).
873 50. Kinsley, C. H. *et al.* Motherhood Induces and Maintains Behavioral and Neural Plasticity
874 across the Lifespan in the Rat. *Arch Sex Behav* **37**, 43–56 (2008).
875 51. Jeffery, K. J. Integration of the sensory inputs to place cells: What, where, why, and how?
876 *Hippocampus* **17**, 775–785 (2007).
877 52. Lisman, J. E. & Grace, A. A. The Hippocampal-VTA Loop: Controlling the Entry of
878 Information into Long-Term Memory. *Neuron* **46**, 703–713 (2005).
879 53. Musser, E. D., Kaiser-Laurent, H. & Ablow, J. C. The neural correlates of maternal
880 sensitivity: An fMRI study. *Dev Cogn Neurosci* **2**, 428–436 (2012).
881 54. Orso, R. *et al.* How Early Life Stress Impact Maternal Care: A Systematic Review of
882 Rodent Studies. *Front Behav Neurosci* **13**, 197 (2019).
883 55. Batt, M. M., Duffy, K. A., Novick, A. M., Metcalf, C. A. & Epperson, C. N. Is Postpartum
884 Depression Different From Depression Occurring Outside of the Perinatal Period? A
885 Review of the Evidence. *Focus (Am Psychiatr Publ)* **18**, 106–119 (2020).

886 56. Neukel, C. *et al.* The maternal brain in women with a history of early-life maltreatment: an
887 imagination-based fMRI study of conflictual versus pleasant interactions with children. *J*
888 *Psychiatry Neurosci* **43**, 273–282 (2018).
889 57. Kim, P. *et al.* Perceived quality of maternal care in childhood and structure and function of
890 mothers' brain. *Dev Sci* **13**, 662–673 (2010).
891 58. Champagne, F. A., Curley, J. P., Keverne, E. B. & Bateson, P. P. G. Natural variations in
892 postpartum maternal care in inbred and outbred mice. *Physiology and Behavior* **91**, 325–
893 334 (2007).
894 59. Anstrom, K. K. & Woodward, D. J. Restraint Increases Dopaminergic Burst Firing in
895 Awake Rats. *Neuropsychopharmacol* **30**, 1832–1840 (2005).
896 60. Heath, F. C. *et al.* Dopamine D1-like receptor signalling in the hippocampus and amygdala
897 modulates the acquisition of contextual fear conditioning. *Psychopharmacology (Berl)* **232**,
898 2619–2629 (2015).
899 61. Espadas, I. *et al.* Dopamine D2R is Required for Hippocampal-dependent Memory and
900 Plasticity at the CA3-CA1 Synapse. *Cerebral Cortex* **31**, 2187–2204 (2021).
901 62. Silva, M. R. P., Bernardi, M. M. & Felicio, L. F. Effects of dopamine receptor antagonists
902 on ongoing maternal behavior in rats. *Pharmacology Biochemistry and Behavior* **68**, 461–
903 468 (2001).
904 63. Numan, M. *et al.* The effects of D1 or D2 dopamine receptor antagonism in the medial
905 preoptic area, ventral pallidum, or nucleus accumbens on the maternal retrieval response
906 and other aspects of maternal behavior in rats. *Behav Neurosci* **119**, 1588–1604 (2005).
907 64. Sariñana, J., Kitamura, T., Künzler, P., Sultzman, L. & Tonegawa, S. Differential roles of
908 the dopamine 1-class receptors, D1R and D5R, in hippocampal dependent memory.
909 *Proceedings of the National Academy of Sciences* **111**, 8245–8250 (2014).
910 65. Grace, A. A. Phasic versus tonic dopamine release and the modulation of dopamine system
911 responsivity: a hypothesis for the etiology of schizophrenia. *Neuroscience* **41**, 1–24 (1991).
912 66. Kroener, S., Chandler, L. J., Phillips, P. E. M. & Seamans, J. K. Dopamine Modulates
913 Persistent Synaptic Activity and Enhances the Signal-to-Noise Ratio in the Prefrontal
914 Cortex. *PLoS One* **4**, e6507 (2009).
915 67. Fadok, J. P., Dickerson, T. M. K. & Palmiter, R. D. Dopamine Is Necessary for Cue-
916 Dependent Fear Conditioning. *J. Neurosci.* **29**, 11089–11097 (2009).
917 68. Wilmot, J. H. *et al.* Phasic locus coeruleus activity enhances trace fear conditioning by
918 increasing dopamine release in the hippocampus. *eLife* **12**, RP91465.
919 69. Kimble, D. P., Rogers, L. & Hendrickson, C. W. Hippocampal lesions disrupt maternal, not
920 sexual, behavior in the albino rat. *Journal of Comparative and Physiological Psychology*
921 **63**, 401–407 (1967).
922 70. Terlecki, L. J. & Sainsbury, R. S. Effects of fimbria lesions on maternal behavior in the rat.
923 *Physiology & Behavior* **21**, 89–97 (1978).
924 71. Froemke, R. C. & Young, L. J. Oxytocin, Neural Plasticity, and Social Behavior. *Annu Rev*
925 *Neurosci* **44**, 359–381 (2021).
926 72. Marlin, B. J., Mitre, M., D'amour, J. A., Chao, M. V. & Froemke, R. C. Oxytocin enables
927 maternal behaviour by balancing cortical inhibition. *Nature* **520**, 499–504 (2015).
928 73. Orchard, E. R. *et al.* The maternal brain is more flexible and responsive at rest: effective
929 connectivity of the parental caregiving network in postpartum mothers. *Sci Rep* **13**, 4719
930 (2023).

74. Champagne, F. A. & Curley, J. P. Plasticity of the Maternal Brain Across the Lifespan: Plasticity of the Maternal Brain Across the Lifespan. *New Directions for Child and Adolescent Development* **2016**, 9–21 (2016).
75. Kempadoo, K. A., Mosharov, E. V., Choi, S. J., Sulzer, D. & Kandel, E. R. Dopamine release from the locus coeruleus to the dorsal hippocampus promotes spatial learning and memory. *Proceedings of the National Academy of Sciences* **113**, 14835–14840 (2016).

Supplementary Materials for

Persistent dopamine-dependent remodeling of the neural transcriptome in response to pregnancy and postpartum

Jennifer C Chan *et al.*

Corresponding author: Ian Maze, ian.maze@mssm.edu

MATERIALS AND METHODS

Animals

Wild-type C57BL6/J mice were purchased from Jackson Laboratories at 8-weeks old, and maintained on a 12-h/12-h light/dark cycle throughout the entirety of the experiments. Mice were provided with *ad libitum* access to water and food throughout the entirety of the experiments. All behavioral testing occurred during the animals' light cycle. Experimenters were blind to experimental group, and the order of testing was counterbalanced during behavioral experiments. All animal procedures were performed in accordance with NIH guidelines and with the approval of the Institutional Animal Care and Use Committee of the Icahn School of Medicine at Mount Sinai.

Breeding

Adult virgin female mice were pair bred in-house with age-matched males. Males were removed after a maximum of 5 days, and pregnant females were singly-housed at least 2 days before parturition. Pups were counted on the day of birth (0 dpp) and weaned at 21 dpp. Only dams with litters between 4-10 pups were used for all experiments. On the day of weaning, dams were group-housed into cages of 3-5 mice with animals of the same experimental condition. For timed breedings, copulation plugs were checked every morning within 1-hour after lights on, where confirmation of a plug was designated as E0.5, signaling the immediate removal of the female to

her own cage with a nestlet. Virgin NP females were age-matched for each experimental cohort. Mating-experienced NP females were confirmed for the presence of a copulation plug. For Pregnancy Only dams, pups were removed at 0 dpp within 3 hours after lights-on to minimize maternal-offspring interactions. For comparison of PP dams to pup sensitized virgin females, litters were culled to 4 pups to equate litter size with the number of pups used for each sensitized female. In all other experiments, litters were not culled.

Postpartum stress paradigm

Stress PP females were subjected to limited nesting and maternal separation from 10-20 dpp, as previously described[1–3]. On each day of separation, the entire litter was removed to a clean cage with Sani-Chip bedding for 3-4 hours. Separations occurred during the light cycle, and the timing varied each day to minimize predictability and acclimatization. EnviroDri nesting material was depleted to 1/3 of control cages during the days of separation. Following pup weaning on 21 dpp, the nesting material was restored to normal levels, and dams were group-housed into cages of 3-5 with animals of the same experimental condition.

Pup sensitization

Pup sensitization was conducted as previously described[4,5]. On the first day of pup sensitization, virgin NP females were presented with four pups (postnatal day 5) from a cage consisting of a lactating donor dam and her litter. Donor pups were exchanged for satiated pups from the same litter every 8-12 hours for 21 days. Donor pups were weighed daily to ensure continual weight-gain throughout the experiment, and only pups that exhibited consistent weight-gain were used. Behavioral observations were conducted during the first four days of sensitization. Each dam was observed for 30 minutes during the light phase for the following maternal behaviors:

1031 licking/grooming, crouching, and nestbuilding. During these observation periods, females were
1032 closely monitored to ensure that they did not display aggressive behavior toward the donor pups.
1033 On the last day of sensitization, donor pups were weaned from the cage, and sensitized females
1034 were group-housed into cages of 3-5 mice with animals of the same experimental condition.
1035
1036 **Brain tissue collections**
1037 Animals were sacrificed by rapid decapitation. Whole brains were flash frozen with cold 2-
1038 methylbutane and stored at −80°C until further processing. Flash-frozen brains were sectioned at
1039 −20°C using a 1 mm mouse coronal brain matrix (Stoelting Co.). Tissues enriched for the brain
1040 region of interest were micropunched using a hollow needle (Ted Pella) according to the Allen
1041 Brain Atlas (see **Fig. S1A**).
1042
1043 **Behavioral analyses**
1044 All animals (18-30 weeks, depending on the time from pup weaning) were handled for 2 minutes
1045 for two consecutive days prior to initial behavioral testing. Animals were habituated to the testing
1046 room for 1 hour prior to each behavioral assay. All testing occurred during the light phase.
1047
1048 *Pup retrieval:* All animals were individually housed for 24-hours prior to testing. Following
1049 habituation, 2 pups from a donor litter with a lactating dam (aged 4-6 dpp) were placed in different
1050 corners opposite to the nest in the home cage. Pup-directed interactions were recorded from above
1051 for 15-minutes or until both pups were successfully retrieved into the nest. Retrieval latency was
1052 calculated as [time pup was first placed into the nest by animal - time first pup was placed into the
1053 cage by experimenter].
1054

1055 *Contextual fear conditioning:* On day 1, mice were habituated for 10 minutes to the testing
1056 chamber, which consisted of a square plexiglass box with a metal grid inside a sound-attenuating
1057 cabinet wiped with 70% ethanol (Med Associates, VT). On day 2, following a 3-minute baseline
1058 measurement, mice were trained with five 2.0-second 0.7 mA foot shocks delivered with an
1059 intertrial interval of 90-seconds. Testing for conditioned fear responses (freezing) for a total of 5-
1060 minutes occurred 24-hours following training. Freezing was measured using ANY-maze software
1061 connected to a camera positioned above the testing chamber. Freezing is expressed as a percentage
1062 of the total test time or as a percentage of the 60-seconds prior to each shock during conditioning.
1063 Animals with freezing levels exceeding 40% prior to the first shock were excluded to remove
1064 potential confounding effects of heightened baseline responsivity that could interfere with
1065 accurately assessing conditioned fear.
1066
1067 *Open Field:* Mice were placed in a 16x16 square arena under dim lighting for 5 minutes. A camera
1068 positioned overhead recorded the total distance and time spent in the center *vs.* periphery using
1069 Ethovision software.
1070
1071 *Object location task:* For training, animals were allowed to freely explore two identical objects
1072 placed equidistant from adjacent corners of a 16x16 cm square arena for 5 or 10 minutes, before
1073 being returned to the home cage. Following a 1-hour delay, the animals were returned to the arena
1074 for testing, during which time one object was moved to the opposing corner. During the test, the
1075 animals were allowed to freely explore the objects for 5-minutes. A camera positioned overhead
1076 recorded time spent exploring each object using Ethovision software. The discrimination score
1077 was calculated as [(time spent with moved object) – (time spent with unmoved object)/[(time spent
1078 with moved object) + (time spent with unmoved object)].

1079
1080 *Light-dark box:* Anxiety-like behavior was tested in an apparatus containing two interconnected
1081 20x20 cm compartments (Omnitech Electronics Inc.). One compartment was illuminated during
1082 the session ("light" side), while the other was covered by an opaque black perspex lid ("dark"
1083 side). The distance, time spent, and number of crossovers in each compartment were automatically
1084 recorded by Fusion software during the 10-minute test.

1085
1086 *Forced Swim Test:* Mice were placed in a 4 liter glass beaker with 2 liters of room temperature
1087 water for 8 minutes. Each session was recorded and scored by a blinded observer. The total number
1088 of seconds that mice were immobile during the last 5 minutes of the test were recorded, as
1089 previously described[6].

1090
1091 *Observation of pup-directed behaviors in the home cage:* Confirmation of maternal behavior in
1092 pup sensitized females was conducted based on prior studies[7]. Animals were observed from the
1093 first to fourth day of pup sensitization, based on published work that maternal sensitization in
1094 C57BL6/J females occurs following 4-days of pup exposures[8,9]. Observations occurred in the light
1095 period in the first 30-minutes after pups were placed in the cage. Each animal was scored every 3-
1096 minutes, with the observed behavior recorded as one or more of the following categories:
1097 nestbuilding, grooming, sniffing, crouching, nursing, eating, drinking, self-grooming, no-contact.
1098 PP dams were scored for the first 4-days following birth (0-3 dpp) concurrently for comparison.

1099
1100 **Estrous cycle testing**

1101 Vaginal samples were taken on each day of behavioral testing. 15 µL of sterile PBS was gently
1102 pipetted into the vagina and mounted on a glass slide. Vaginal smears were stained with crystal
1103 violet dye, washed twice with water, and cover slipped with glycerol. Three 20x images per sample

1104 were acquired on a light microscope. Estrous stage was determined using the pretrained network
1105 of EstrousNet[10], and confirmed afterwards by a trained experimenter based on cytology of
1106 nucleated, cornified, or leukocytic cells.
1107
1108 **Viral Transduction**
1109 Mice were anesthetized with ketamine (100mg/kg) and xylazine (10 mg/kg) i.p. and positioned in
1110 a stereotaxic frame (Kopf instruments). Given the widespread changes in dopamine receptor
1111 expression across dHpc subregions, we did not restrict our viral manipulations to a specific
1112 subregion. 2 µl of retrograde AAV.rTH.PI.Cre.SV40 (titer ≥ 7×10^{12} vg/mL, Addgene #107788-
1113 AAVrg) was infused bilaterally into the dHpc at 0.2 uL/min using the following coordinates: 7°
1114 angle; anterior-posterior (AP) -2.2 mm, medial-lateral (ML) ±2.0 mm, dorsal-ventral (DV) -2.0
1115 mm. 1 µl of pAAV-hSyn-DIO-mCherry (titer ≥ 4×10^{12} vg/mL, Addgene #50459-AAV2) or
1116 pAAV-hSyn-DIO-hM4D(Gi)-mCherry (titer ≥ 5×10^{12} vg/mL; Addgene #44362-AAV2) was
1117 bilaterally infused into the VTA using the following coordinates: 7° angle; AP -3.3 mm, ML ±0.9
1118 mm; DV -4.6 mm. Needles remained in place for 7 minutes following injection to minimize virus
1119 diffusion. Viral validations were conducted at least 21 days post-surgery to allow for optimal viral
1120 expression and recovery.
1121
1122 **Chemogenetic manipulation**
1123 To directly manipulate dopamine signaling in dHpc, we selectively targeted the VTA-dHpc
1124 projection during a window established as being critical for dopaminergic downregulation.
1125 Following 7 days of recovery, surgerized female mice were randomly assigned to NP or PP groups.
1126 PP females were pair bred with naïve male mice for a maximum of 5 days, and individually housed
1127 prior to parturition. From 10-20 dpp, PP females were injected subcutaneously with

1128 deschloroclozapine (DCZ, Tocris #7193) – to minimize off-target effects[11] - at 1ug/kg in 1%
1129 DMSO or vehicle (saline). NP females were injected with DCZ concurrently. Following weaning
1130 on 21 dpp, PP dams were group-housed with animals of the same experimental condition.
1131 Behavioral testing occurred beginning at 28-days post-weaning (49 dpp), and brain tissues were
1132 collected following contextual fear conditioning for further analyses.
1133
1134 **RNAscope in situ hybridization and analysis**
1135 Fresh frozen brains were cut into 12-16 µm thick slices in the coronal plane with a cryostat (Leica
1136 CM3050-S), mounted on charged Superfrost Plus microscope slides (Thermofisher #P36934), and
1137 stored at -80°C until processing. Sections were post-fixed with 4% PFA for 1.5 hours at 4°C, and
1138 permeabolized with hydrogen peroxide (10 minutes RT) and Protease III (30 minutes RT). The
1139 RNAscope Multiplex Fluorescent Reagent Kit v2 (ACD Bio) was used according to
1140 manufacturer's instructions to sequentially stain sections with the following probes: Drd1a (Mm-
1141 Drd1a-C1, #461901) and Drd2 (Mm-Drd2-C3, #406501-C3). RNAscope probes were visualized
1142 using TSA Vivid Fluorophores (Tocris) at 1:750 dilution. Sections were counterstained with DAPI
1143 (ACD Bio) and mounted using ProLong Gold Antifade Mountant (Thermo). Confocal images (3
1144 images per animal, 1024 × 1024 pixels) were acquired on a Zeiss LSM 780 upright microscope
1145 using a 40X objective with Zen Black software, with 5x1 tiled images. Images were averaged
1146 across 8 consecutive acquisitions at a bit depth of 16 bits, with 2 z-stacks acquired per image.
1147 Subcellular quantification of individual puncta per 100 µm nucleus - identified by cellular
1148 detection of DAPI staining - was performed for each maximum intensity projected image using
1149 QuPath software (v.0.5.1)[12]. Regions of interest (CA1 and dentate gyrus) were annotated and
1150 determined by superimposing images onto the Allen Brain Atlas.
1151

1152 **Immunofluorescence and analysis**

1153 Mice were anesthetized with isoflurane and perfused with cold 1×PBS followed by 4% PFA.
1154 Brains were post-fixed in 4% PFA overnight and then transferred to a 30% sucrose/PBS solution
1155 for 2 days. Brains were sectioned at 40 µm thickness using a Leica CM3050-S cryostat, with serial
1156 sections collected from the VTA. For each subject, 2–3 brain slices were blocked for 2 hours (0.1%
1157 Triton X-100, 10% normal donkey serum), followed by overnight incubation at 4 °C with primary
1158 antibodies: chicken anti-tyrosine hydroxylase (1:500, Aves Labs #TYH) and rabbit anti-Fos
1159 (1:2000, Synaptic Systems #226-008). The next day, slices were incubated for 2 hours at RT with
1160 fluorescent-conjugated secondary antibodies (donkey anti-chicken Alexa Fluor 488, Invitrogen
1161 #A78948; donkey anti-goat Alexa Fluor 680, Invitrogen #A10043). Slices were counterstained
1162 with DAPI (1:10000, Thermo Scientific #62248) and mounted with ProLong Gold Antifade
1163 Mountant (Thermo Fisher #P36934). Confocal images (2-3 replicates per animal, 1024 x 1024
1164 pixels) were acquired on a Zeiss LSM 780 upright microscope using a 40x objective with Zen
1165 Black software. Images were averaged across 8 consecutive acquisitions at a bit depth of 16 bits.
1166 Image analysis was conducted using FIJI software (NIH). The Fos and TH channels were
1167 thresholded using the MaxEntropy method to define regions of interest. Following identification
1168 of colocalized Fos+/TH+ signal, Fos intensity was measured and averaged from 4-6 images per
1169 animal. Brightness and contast were adjusted for representative images.

1170
1171
1172 **Dopamine ELISA**

1173 Brain tissue dopamine levels were assessed in response to 3 hours of pup separation in the home
1174 cage. Independent biological replicates were collected at each time point, with separate animals
1175 used for each measurement. Brains were rapidly harvested (see Brain Tissue Collection, above) at

1176 baseline (prior to pup removal, 0 min), during pup removal (30 and 180 min), and 30 min after
1177 pups were returned to the home cage (210 min). For assessment of NP females, samples were
1178 collected in the home cage 30-min following removal of a littermate. Equal weights of
1179 micropunched brain tissues were homogenized in lysis buffer (0.01 N HCl, 1 mM EDTA, 4 mM
1180 sodium metabisulfite). Tissue dopamine levels were assessed using the Dopamine (Research)
1181 ELISA Kit (ALPCO Diagnostics) according to manufacturer's instruction.

1182

1183 **HPA axis assessment**

1184 Plasma corticosterone levels were assessed in response to 3-hours of pup separation in the home
1185 cage. Testing was initiated within 2-hours after lights on. Tail blood was collected prior to pup
1186 removal (0 min), during pup removal (30 and 180 min), and 120 min after pups were returned to
1187 the cage (300 min). Samples for control animals in the home cage, used to account for the effects
1188 of handling-induced stress, were collected concurrently. Blood samples were immediately mixed
1189 with 50 mM EDTA and centrifuged at 5000 rpm for 10 minutes. Plasma was collected and stored
1190 at −80 °C until analysis. Corticosterone levels were quantified using a Corticosterone ELISA kit
1191 (ENZO Life Sciences) according to manufacturer's instruction.

1192

1193 **Statistics**

1194 Statistical analyses for behavioral and immunoassay data were conducted using Prism software
1195 (GraphPad, v.10.4.1). For experiments involving multiple conditions, one-way or two-way
1196 ANOVAs were performed, followed by *post hoc* analyses when appropriate. For time course
1197 analyses where multiple measurements were taken from the same animal, repeated measures
1198 ANOVAs were performed. Two-tailed Student's t-tests were used for comparisons between two
1199 conditions. Behavioral data derived from manual observations and pregnancy/litter outcomes were

1200 analyzed using chi-square tests. Grubb's test (alpha = 0.05) was applied to detect outliers where
1201 necessary. Statistical significance was defined as $p \leq 0.05$.
1202
1203 **Bulk RNA-seq and analysis**
1204 *RNA isolation and library preparation:* Total mRNA was extracted from frozen brain tissues after
1205 homogenization in Trizol Reagent (Thermo Fisher) and cleaned using RNeasy Microcolumns
1206 (Qiagen) following the manufacturer's instructions. For RNA-seq library preparation, 150 ng of
1207 mRNA per sample was used with either the Illumina Stranded mRNA Prep Kit (Illumina,
1208 #20040534) or the TruSeq RNA Library Prep Kit v2 (Illumina, #RS-122-2001), according to the
1209 manufacturer's protocols. Library quality was assessed using a Qubit Fluorometer 2.0 (Thermo
1210 Fisher) and a High Sensitivity D5000 TapeStation assay (Agilent) before sequencing on a NovaSeq
1211 6000 or NovaSeq X system.
1212
1213 *Differential expression analysis:* Raw fastq files, containing an average of 20–30 million reads per
1214 sample, were processed for pseudoalignment and abundance quantification using Kallisto (v.
1215 0.46.1) against the Ensembl Mus musculus reference (v. 79)[13]. To filter lowly-expressed genes,
1216 only those with a total read count of at least 10 across all samples were retained. To account for
1217 unwanted variation among samples within each sequencing experiment that could arise from
1218 technical or biological factors unrelated to the conditions of interest (including litter size, estrous
1219 stage, day of sample collection, etc.), RUVs (v1.32.0) was applied with a negative control gene set
1220 derived from the total genes identified per sequencing experiment, after ensuring that unwanted
1221 variation did not correlate with covariates of interest, as described previously[14,15]. Differential
1222 expression analysis was performed using DESeq2 (v1.38.3)[16], with significant genes defined by
1223 an adjusted p-value < 0.05. For brain-wide transcriptome comparisons in which samples were

1224 processed across multiple sequencing runs and stemming from separate cohorts, pairwise
1225 comparisons were performed independently for each brain region. For all other experiments, where
1226 subjects came from the same cohort and were processed in a single sequencing run, all groups
1227 were analyzed together to maintain consistent normalization within the experiment. Gene
1228 expression time course analyses examining the periods before, during, and after pregnancy and
1229 postpartum were performed on normalized count data using the ImpulseDE2 package (v0.99.10)[17]
1230 for each brain region. Significant genes exhibiting transient regulation or monotonous changes in
1231 expression were identified using case-only differential expression analysis, with a Q-value
1232 threshold of 0.05.
1233
1234 *Weighted gene co-expression analysis:* To identify brain-wide gene co-expression networks,
1235 normalized count data for all brain regions were compiled and analyzed using the WGCNA
1236 package (v1.73)[18]. Co-expression networks were constructed from the 7,500 most variable genes,
1237 determined by ranking gene variance. A soft threshold power of 12 was identified with the
1238 pickSoftThreshold function to ensure scale-free network properties. Modules were identified
1239 based on dissimilarity of a signed topological overlap matrix (TOM), and named with an arbitrary
1240 color. The "gray" module encompassed genes that did not segregate into any specific module, and
1241 was therefore removed from further analyses. To assess the enrichment of differentially expressed
1242 genes (DEGs) within each brain region per module, Fisher's exact tests were performed using the
1243 fisher.test() function in R (v4.3.0). To analyze the correlation between gene modules and brain
1244 regional sensitivity to parity, brain regions were categorized into two groups based on the top five
1245 regions with significant DEG overlap. These regions were designated as "High Sensitivity"
1246 regions, while all other regions were classified as "Low Sensitivity." Pearson correlation
1247 coefficients were calculated to examine the relationship between each module and the trait

1248 (regional sensitivity × parity status), with statistical significance determined by Student's t-tests (p
1249 <0.05). Heatmaps were generated to visualize these module-trait correlations, and module-specific
1250 gene lists were exported for pathway enrichment analysis.
1251
1252 *Pathway and predicted upstream regulator analyses:* Functional annotation of DEGs was
1253 conducted using ShinyGO (v0.81)[19], with all protein-coding genes in the mm10 genome used as
1254 the background. Pathways with an FDR < 0.05 were considered significant. All significant
1255 pathways and associated statistics are provided in the Supplementary Tables. For figures, relevant
1256 pathways were selected from the top 10 or 1/3 of significant terms, ranked by FDR, to emphasize
1257 processes consistent with hypotheses informed by published literature. For GO term selection,
1258 Revigo[20] was used to reduce redundancy of overlapping GO terms when needed. Ingenuity
1259 Pathway Analysis (IPA; Qiagen, Inc., v.01-23-01) was used to predict upstream regulators for
1260 DEG lists[21]. For "High Sensitivity" and "Low Sensitivity" regions (see *WGCNA* section), DEGs
1261 shared by at least two or three brain regions were extracted, irrespective of the direction of change.
1262 The IPA software was used to identify upstream regulators associated with each DEG list, with
1263 statistical significance defined as p < 0.05. To investigate the mechanisms underlying parity
1264 programming of dHpc plasticity, significant upstream regulators were systematically prioritized
1265 based on one or more of the following criteria: (1) multiple molecules involved in the same
1266 signaling pathways (e.g., progesterone and its receptor, PGR); (2) structurally similar molecules
1267 that engage analogous signaling cascades (e.g., levodopa and dopamine); (3) molecules known to
1268 be influenced by reproductive exposures; (4) molecules demonstrated to play a role in hippocampal
1269 plasticity; (5) molecules identified as significant in both "High Sensitivity" and "Low Sensitivity"
1270 regulator lists; and (6) molecules with high statistical significance values. Following selection,
1271 upstream regulators were categorized into general molecular classes (e.g., "Hormone,"

1272 "Transcription Factor," "Lipid") and grouped for visualization. Data are presented as a bubble plot,
1273 with marker shape representing number of brain regions sharing DEGs and marker size
1274 corresponding to significance.
1275
1276 *Gene expression overlap analyses:* Jaccard indices were calculated for overlapping gene lists using
1277 the GeneOverlap package (v1.36.0)[22], with significance defined by $p < 0.05$. Fisher's exact tests
1278 were calculated using the base *fisher.test()* function in R (v. 4.3.0) following construction of
1279 contingency tables for each comparison. Transcriptome-wide, threshold-free gene expression
1280 overlap was visualized using Rank-Rank Hypergeometric Overlap (RRHO) heatmaps generated
1281 with the RRHO2 package (v1.0)[23]. Gene lists were ranked by signed p-values, calculated as the
1282 log10-transformed nominal p-value multiplied by the sign of the fold change, without applying
1283 differential expression thresholds.
1284
1285 *Cell-type deconvolution:* Brain cell-type proportion was estimated from normalized expression
1286 data using the BRETIGEA package (v.1.0.4)[24] with default markers. For comparisons between
1287 groups, surrogate proportion variables were normalized using the Normalize function in Prism
1288 (GraphPad, v. 10.4.1). Each sub column was normalized separately, with the smallest value set to
1289 0% and the largest value set to 100%. To calculate $\log_2$(fold change) between groups, normalized
1290 values per cell-type per group were averaged and expressed as the log2 ratio of the group means.
1291
1292 **Single nuclei RNA-seq**
1293 *Nuclei isolation and library preparation:* For each animal, 2 mm dHpc-enriched tissue
1294 micropunches were collected bilaterally from consecutive 1 mm slices from -0.80 to -2.80 mm
1295 relative to bregma for a total of 4 punches (Ted Pella). Samples were processed in batches of 4-6,
1296 with each group represented within each batch. Nuclei were isolated using a modified version of

1297 a sucrose density gradient isolation protocol[25]. Briefly, thawed tissues were placed in 1 mL of lysis
1298 buffer (0.32 M sucrose, 5 mM $CaCl_2$, 3 mM magnesium acetate, 0.1 mM EDTA, 10 mM Tris-HCl
1299 pH 8, 1 mM DTT, 0.1% Triton X-100) with 50 µL of 25 U/mL RNase inhibitor (Takara #2313B)
1300 in a dounce homogenizer (Wheaton #357538). Homogenization was performed with 20 strokes
1301 using a tight pestle. Another 1 mL of lysis buffer was added, followed by an additional 10 strokes.
1302 The resulting 2 mL homogenate was transferred to a 15 mL Open-Top Thinwall Polypropylene
1303 Tube (Beckman-Coulter #361707). The homogenizer and pestle were rinsed with 2 mL of lysis
1304 buffer, and this wash was combined with the homogenate for a total of 4 mL. The homogenate
1305 was carefully underlaid with 9 mL of sucrose solution (1.8 M sucrose, 3 mM magnesium acetate,
1306 1 mM DTT, 10 mM Tris-HCl pH 8) and ultracentrifuged at 24,000 rpm for 1 hour at 4 °C using a
1307 Sorvall™ WX+ centrifuge. After centrifugation, the supernatant and debris at the interface were
1308 gently removed. The nuclear pellet was resuspended in 1 mL of resuspension buffer (0.02% bovine
1309 serum albumin in DPBS with 25 µL of 25 U/mL RNase inhibitor) and incubated on ice for 10
1310 minutes. The suspension was passed through a 35 µm nylon mesh filter (Corning #352235) into a
1311 1.5 mL RNase/DNase-free microcentrifuge tube and centrifuged at 2600 x g for 10 minutes at 4
1312 °C. Supernatants were discarded, and nuclei were resuspended in 200 µL of resuspension buffer.
1313 A 10 µL aliquot of the nuclei suspension was stained with Trypan Blue to assess quality and
1314 concentration using a Countess 3 Automated Cell Counter. Nuclei suspensions were loaded onto
1315 a Chromium Single Cell 3′ chip (10X Genomics, v3) and processed according to the manufacturer's
1316 protocol, targeting 10,000 nuclei. Single-nuclei libraries were generated using the 10X Chromium
1317 Next GEM Single Cell 3′ v3.1 (Dual Index) protocol (CG000315 Rev A). Libraries were pooled,
1318 loaded onto a single 10B 100 Cycle Flowcell, and sequenced using an Illumina NovaSeq 6000
1319 system to generate 25-30,000 paired-end 2 × 100 bp reads.

1320
1321 *Data analysis:* FastQ files were processed with the 10X Genomics Cell Ranger pipeline (v7.1.0)
1322 to demultiplex reads, align them to the mouse genome (mm10-2020-A), remove PCR duplicates,
1323 and generate gene expression matrices. Cell Ranger filtered outputs were analyzed using Seurat
1324 v4.3.0[26], and mitochondrial RNA content per cell was calculated using the GRCm39 (mm10)
1325 genome annotation and regressed out using SCTransform normalization protocol included in the
1326 Seurat toolkit with 20 principal components (PCs) and a resolution of 0.1. To estimate ambient
1327 RNA and correct for background contamination, the SoupX (v1.6.2) package[27] was used for each
1328 sample using raw and filtered feature matrices from the Cell Ranger output. Heterotypic doublets
1329 were identified and removed using DoubletFinder (v2)[28] to ensure the integrity of singlet datasets.
1330 Filtered singlet datasets were then re-normalized and integrated using the same Seurat
1331 SCTransform v2 workflow mentioned above. Cell clusters were annotated using a combination of
1332 expert curation based on published marker genes[29–35], and label transfer from hippocampal
1333 reference datasets, including the Allen Brain Map and Broad Institute resources[34,36]. Clusters with
1334 contaminant cell populations expressing markers for choroid plexus (*Ttr*), ependymal (*Tmem212*),
1335 and vascular leptomeningeal cells (*Vtn, Col1a2*) were removed from the analysis[35,37–39].
1336 Additionally, as the sequential 2mm micropunches encompassed portions of cortical, thalamic and
1337 vHpc regions, clusters characterized by enrichment of published non-dHpc neuronal markers using
1338 Seurat's FindMarkers function (layer 5/6 cortical: *Rorb, Foxp2*[39]; ventral granule neurons: *Tox3*[31])
1339 were also removed from the analysis. Cell cluster proportion analyses were conducted using the
1340 scProportionTest package[40], which employs a Monte Carlo permutation test to evaluate whether
1341 observed differences result from random sampling. Proportional differences between conditions
1342 were compared to a null distribution generated by resampling, and statistical significance was
1343 determined by permutation-based p-values with confidence intervals estimated via bootstrapping.

1344 Differential expression analysis was conducted using pseudobulk analysis, where gene counts
1345 were summed across all cells within each sample for each cell type cluster using the
1346 AggregateExpression() function. DESeq2 was then applied at the sample level to conduct
1347 differential expression. To explore pathways underlying cluster-specific differences across
1348 conditions, pathway analysis was conducted using ShinyGO on genes meeting the following
1349 criteria: $\log2FC > 1.5$ and $p < 0.05$.

1350

1351 **DATA AND MATERIALS AVAILABILITY**

1352 The RNA-seq data generated in this study have been deposited in the National Center for
1353 Biotechnology Information Gene Expression Omnibus (GEO) database under accession numbers
1354 GSE289991 and GSE289992. We declare that the data supporting findings for this study are
1355 available within the article and Supplementary Information. Related data are available from the
1356 corresponding author upon reasonable request. No restrictions on data availability apply.

1357

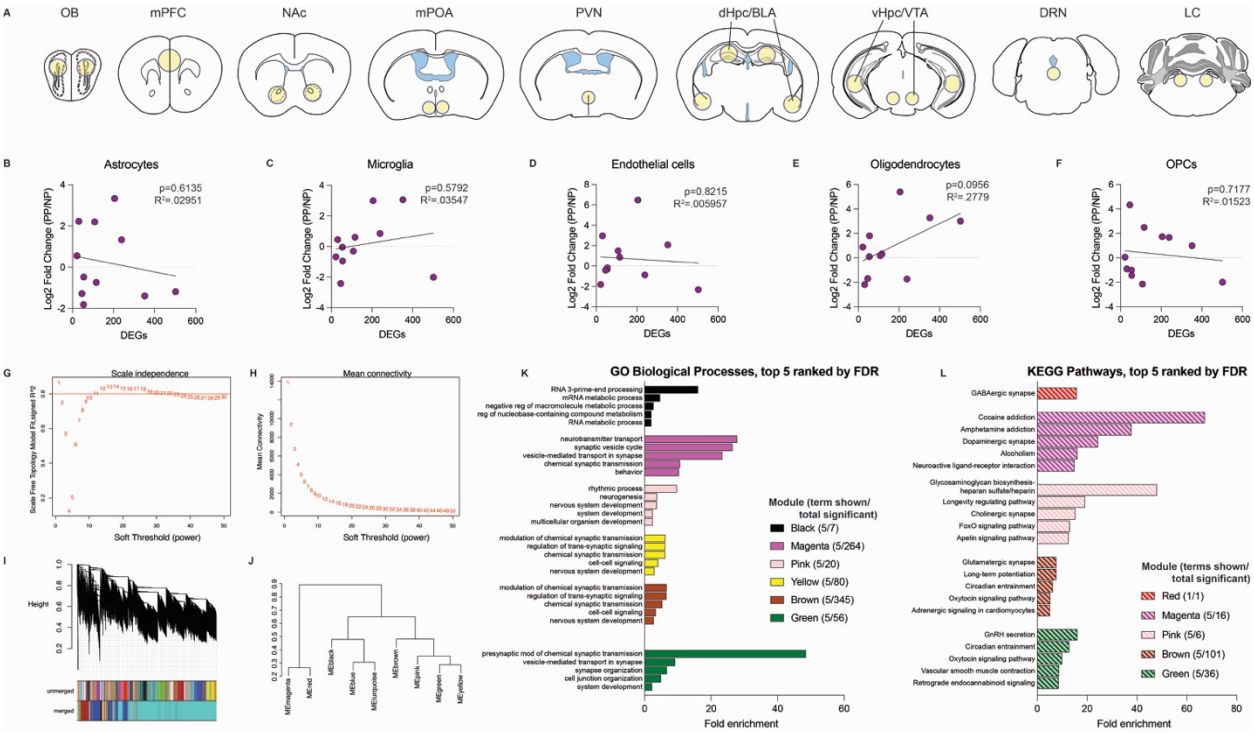

Figure S1: Brain-wide transcriptomic analysis of cell markers and gene expression networks. A) Brain regions selected for bulk transcriptional profiling: olfactory bulb (OB), medial prefrontal cortex (mPFC), nucleus accumbens (NAc), medial preoptic area (mPOA), paraventricular nucleus (PVN), dorsal hippocampus (dHpc), basolateral amygdala (BLA), ventral hippocampus (vHpc), ventral tegmental area (VTA), dorsal raphe nucleus (DRN), and locus coeruleus (LC). Yellow circles indicate area selected for tissue micropunching. **B-F)** Nonsignificant correlations between the fold change (NP *vs.* PP) in normalized surrogate proportion variables generated from cell-type deconvolution of bulk RNA-seq data for **B)** astrocytic, **C)** microglia, **D)** endothelial, **E)** mature oligodendrocyte, and **F)** oligodendrocyte precursor cell markers with the number of DEGs identified from each brain region. **G)** Scale independence plot for soft-threshold power selection for WGCNA analysis, illustrating the relationship between β and the scale-free topology fit index, identifying the optimal β value = 12. **H)** Mean connectivity plot illustrating the average network density for each evaluated soft-thresholding power. **I)** Dendrogram of gene clustering based on topological overlap, highlighting the hierarchical clustering process used for module detection and merging of similar modules. **J)** Dendrogram of eigengene network adjacency depicting similarity of modules. **K, L)** Significantly enriched **K)** GO Biological Processes and **L)** KEGG pathways, sorted by FDR values, from module gene sets. Bars are color-coded to indicate modules. The total number of significant terms for each analysis is provided.

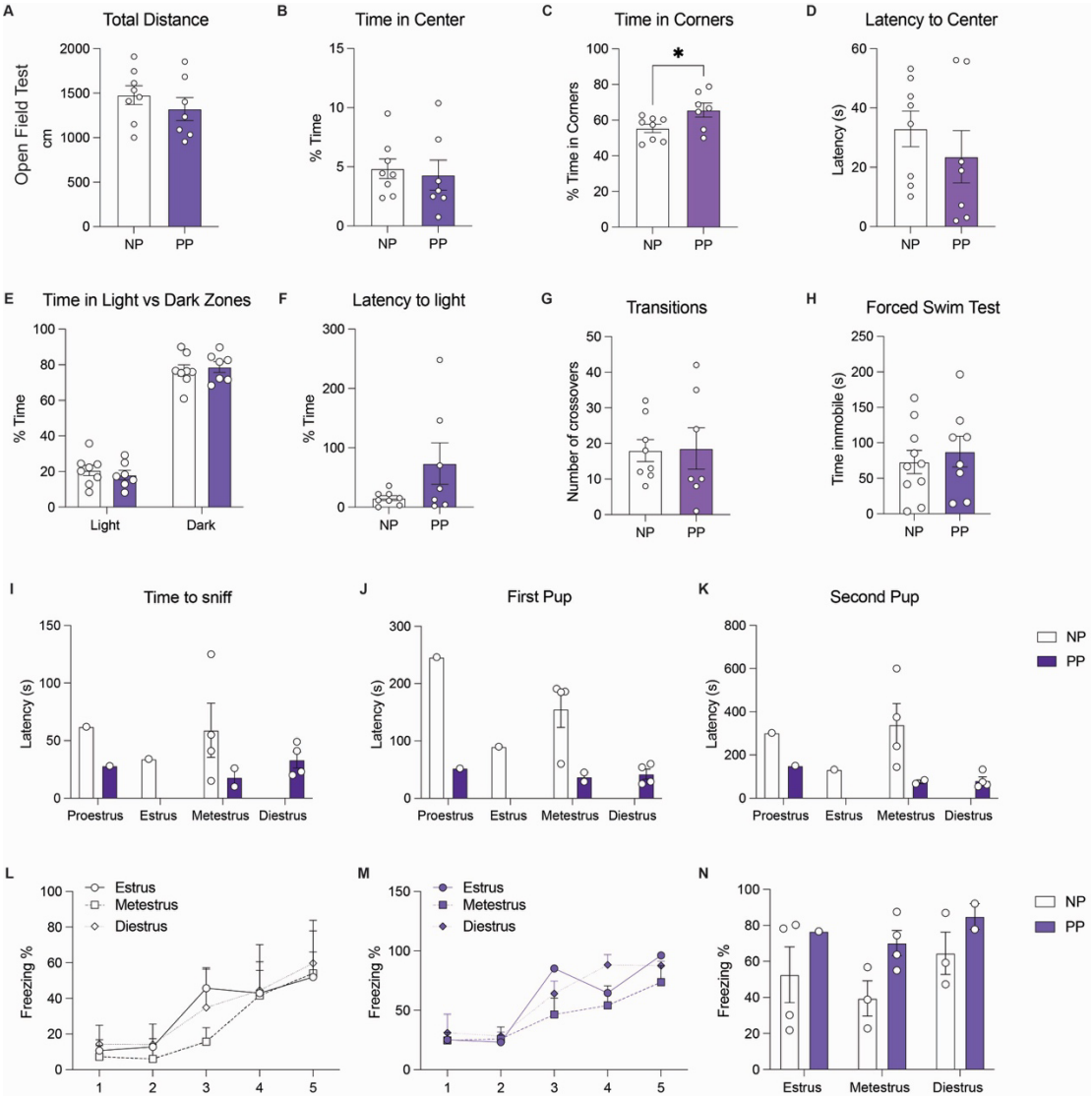

Figure S2: Parity associated behavioral adaptations are not influenced by locomotion, anxiety-/depressive-like behaviors, or estrous stage. A-D) In the open field test, there was no change in total distance, time spent in the center, or latency to the center. While there was a significant increase in time spent in corners for PP dams (Student's t-test, $t(13) = 2.307$, $*p = 0.0382$), this did not impact any other outcomes on the open field test. **E-G)** In the light-dark box, there was no difference in time spent in lights *vs.* dark zones, latency to enter the light zone, or transitions between zones. **H)** There was no difference in time spent immobile on the forced swim test. **I-K)** Stratification of pup retrieval behaviors by estrous stage on the day of testing did not reveal a significant effect of estrous stage. **L-N)** Similarly, stratification of contextual fear conditioning outcomes did not identify a significant effect of estrous stage on acquisition or context recall in NP or PP groups. Error bars represent mean ± SEM. N=6-11 animals/group.

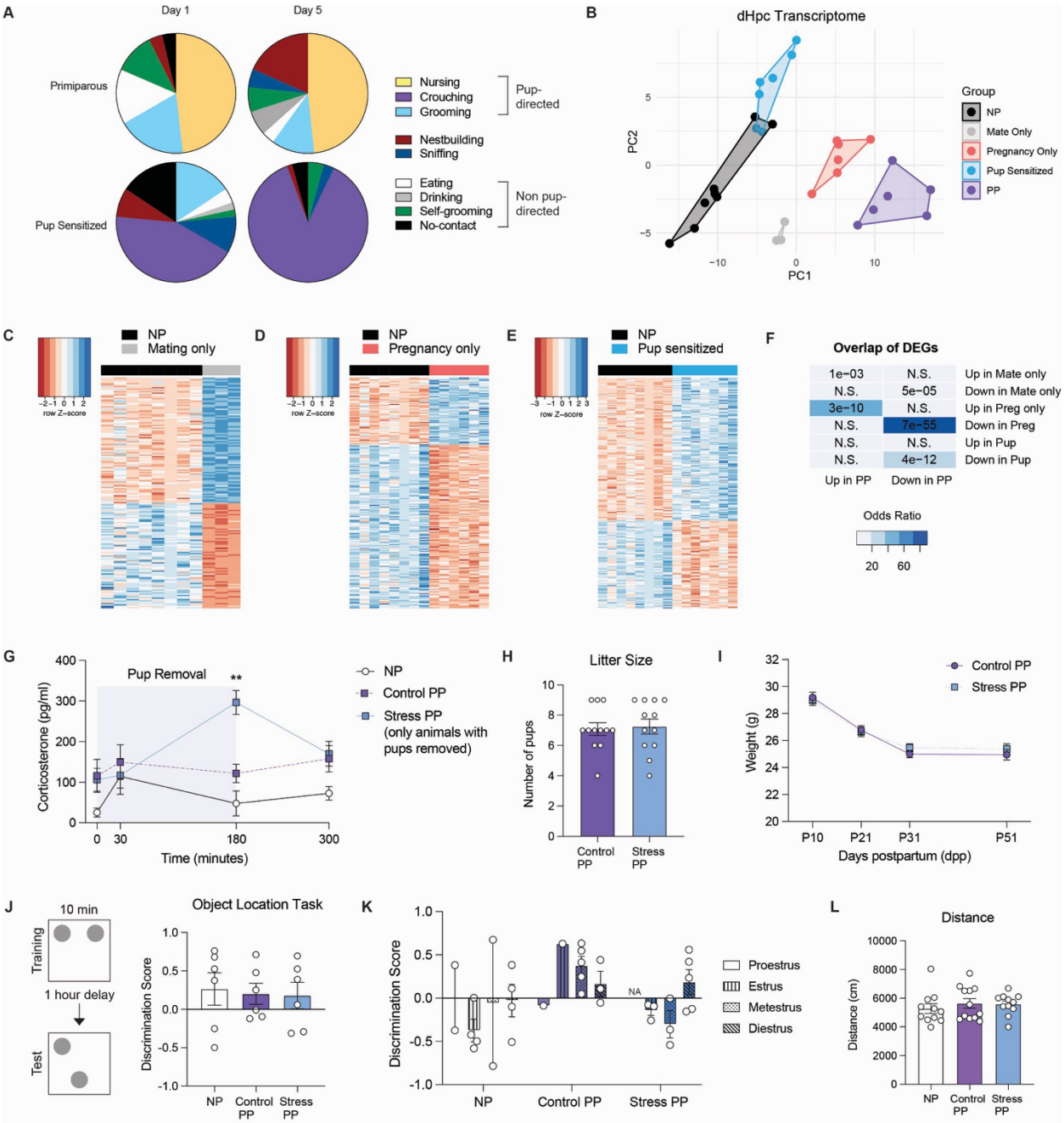

Figure S3: Postpartum experiences modulate the extent of parity-associated dHpc transcriptomic and behavioral adaptations. A) Pie charts showing significant shifts towards pup-directed behaviors, representing maternal behavior initiation after four days of pup exposure in Pup Sensitized virgin females ($\chi^2(7) = 33.52$, $p = 2.11 \times 10^{-5}$). **B)** Principle components analysis of NP *vs.* PP DEGs (adj $p < 0.05$) from dHpc, showing the Pregnancy Only group clusters most closely with PP. **C)** Heatmaps of all significant DEGs comparing NP *vs.* Mating only, **D)** NP *vs.* Pregnancy only, **E)** NP *vs.* Pup sensitized dHpc transcriptomes. **F)** Odds ratio analysis of DEG overlap for all comparisons (*vs.* NP). Insert numbers indicate respective *p* values for each association (N.S., $p > 0.05$). **G)** Pup separation increases maternal corticosterone levels over 3-

hours (RM two-way ANOVA, group: $F(2,15) = 12.86$, $p = 0.0006$, time: $F(2.125, 31.87) = 2.759$, $p = 0.0756$, interaction: $F(6,45) = 3.294$, $p = 0.009$; Tukey's multiple comparisons test: Control *vs.* Stress PP, $^{**}p < 0.01$). N = 6 animals/group. **H)** No effect of postpartum stress on litter size. N = 12/group. **I)** Postpartum stress did not alter maternal weights. **J)** All groups discriminated the novel location following 10-minutes of training on the object location task (one way ANOVA, $F(2,15) = 0.06452$, $p = 0.9378$) N=6 animals/group. **K)** Stratification of object location test scores did not show a significant effect of estrous stage. **L)** There was no difference in the total distance travelled in the open field test across groups. Error bars represent mean ± SEM.

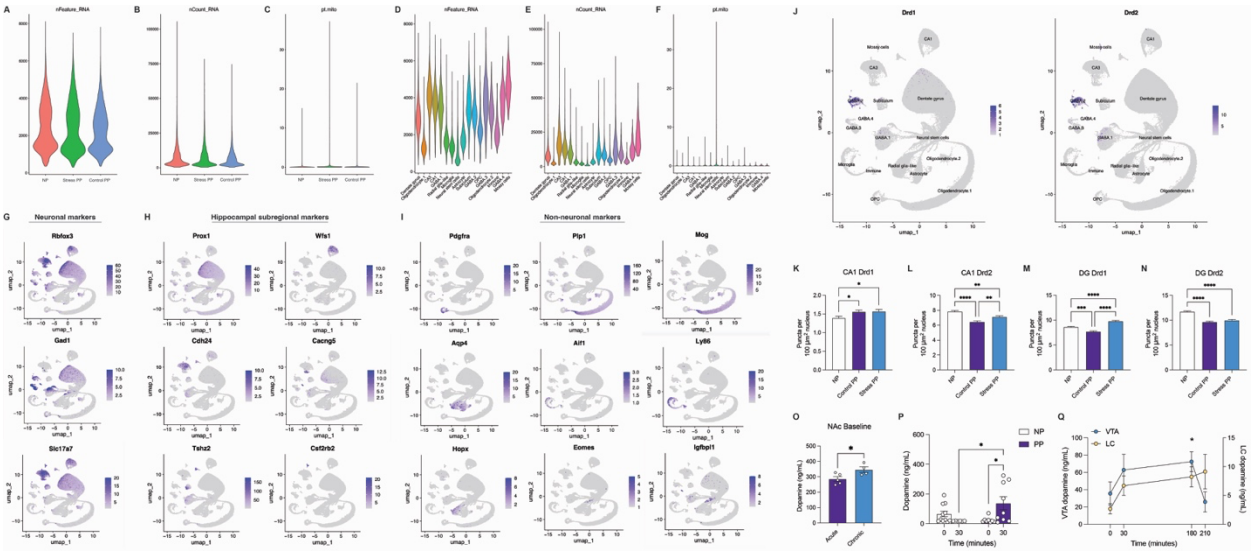

Figure S4: snRNA-seq quality control assessments, cell marker gene expression, and postpartum dopamine modulation. Violin plots showing the **(A)** number of detected genes, **(B)** UMI number, and **(C)** mitochondrial gene % by group following regression for mitochondrial gene mapping. (**D-F)** Breakdown of these metrics by annotated clusters show <10% mitochondrial gene across all cell-types, except for a minority of neural stem cells. Unsupervised clustering of snRNA-seq data with cells colored for **(G)** neuronal, excitatory, and inhibitory markers; **(H)** hippocampal subregional markers; and **(I)** non-neuronal markers including for glial and neural progenitor populations. **J)** Unsupervised clustering of snRNA-seq data with cells colored for *Drd1* (left) and *Drd2* (right) expression. **K)** Quantification of *Drd1* mRNA puncta in CA1 nuclei (one-way ANOVA, ($F(2,19204) = 3.963$, $p = 0.019$). **L)** Quantification of *Drd2* mRNA puncta in CA1 nuclei (one-way ANOVA, ($F(2,19204) = 23.16$, $p < 0.0001$). **M)** Quantification of *Drd1* mRNA puncta in dentate gyrus nuclei (one-way ANOVA, ($F(2,21864) = 42.09$, $p < 0.0001$). **N)** Quantification of *Drd2* mRNA puncta in dentate gyrus nuclei (one-way ANOVA, $(2,21864) = 41.79$, $p < 0.0001$). Tukey's multiple comparisons test, *$p < 0.05$, **$p < 0.01$, ***$p < 0.001$, ****$p < 0.0001$. **O)** Chronic postpartum stress resulted in higher baseline levels of dopamine in the nucleus accumbens (NAc; Student's t-test, $t(7) = 2.568$, *$p = 0.0371$). N= 4-5 animals/group. **P)** Dopamine response is not induced in NP dHpc 30-minutes following littermate separation (two-way ANOVA, interaction of time x group ($F(1,30) = 8.78$, $p = 0.0059$, time ($F(1,30) = 1.47$, $p = 0.2359$, group, ($F(1,30) = 2.054$, $p = 0.1621$); Tukey's multiple comparisons test, *$p < 0.05$). N = 6-11 animals/group. **Q)** Dopamine levels increased during pup separation in the VTA (left y-axis), but not in the locus coeruleus (right y-axis), resembling patterns of NAc and dHpc dopamine dynamics (two-way ANOVA, effect of brain region ($F(1,46) = 32.32$, $p < 0.0001$), time ($F(3,46) = 2.311$, $p = 0.0866$), interaction ($F(3,46) = 1.118$, $p = 0.1109$); Dunnett's multiple comparisons test, *$p < 0.05$). N = 5-8 samples/group. Error bars represent mean ± SEM.

1442

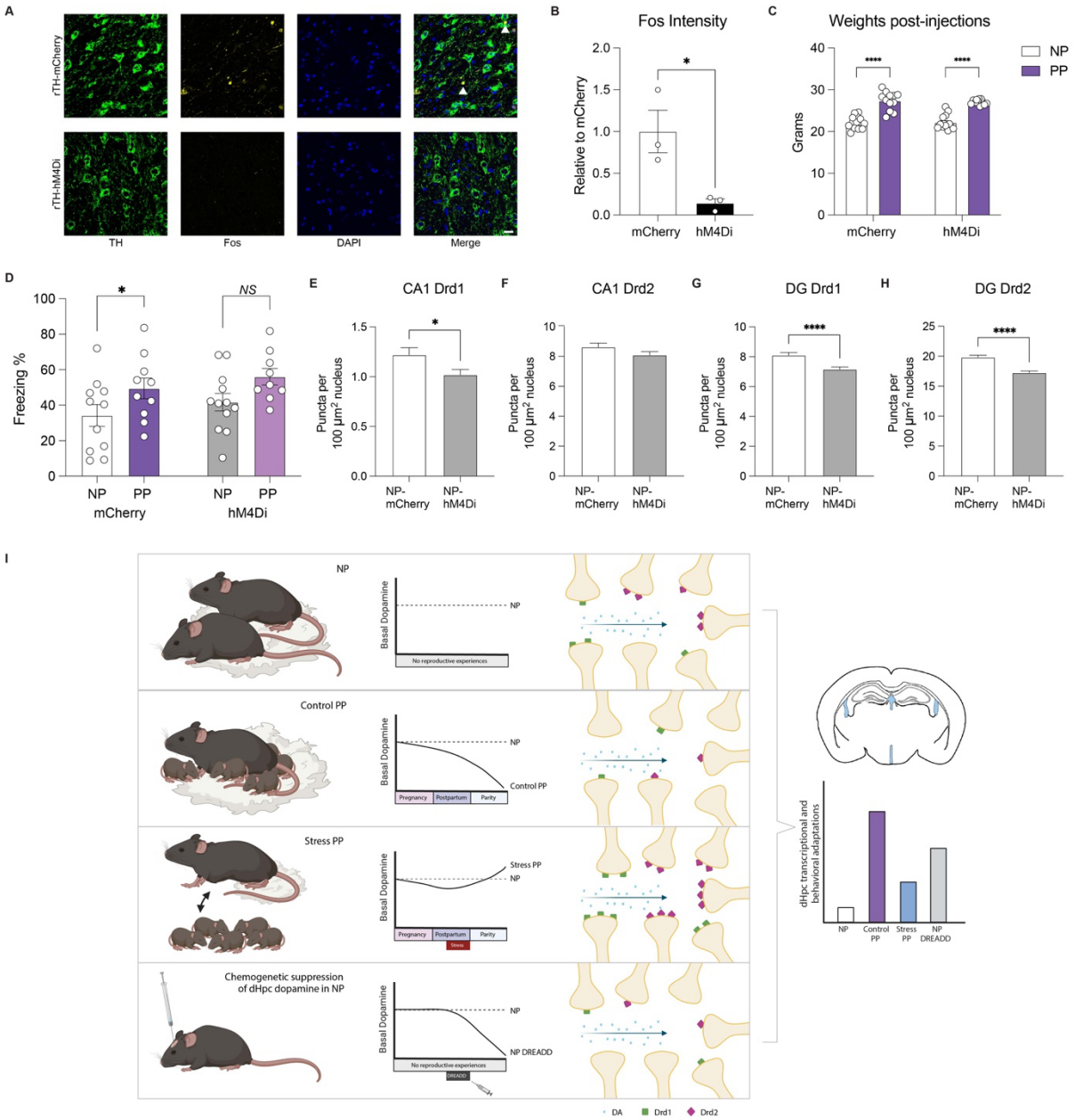

1443
1444

1445 **Figure S5. Inhibition of VTA-dHpc projection mimics sustained changes in dopamine**
1446 **receptor dynamics. A)** Representative images of c-Fos immunostaining in the VTA. Scale bars,
1447 20 µm. **B)** Quantification of c-Fos immunoreactivity in VTA TH+ neurons (Student's t-test; t(4)
1448 = 3.299, *p = 0.03). N = 3 animals/group. **C)** Chronic DCZ injections did not alter weights at 21
1449 dpp (two-way ANOVA; main effect of group (F(1,48) = 128, p < 0.0001), virus (F(1,48) = 0.0862,
1450 p = 0.7702); Tukey's multiple comparison's test, ****p < 0.0001). **D)** Parity induced significantly
1451 greater freezing on the context recall text in mCherry dams, with trending effects between hM4Di
1452 groups (two-way ANOVA (effect of group, (F(1,38) = 7.177, p = 0.0109, virus (F(1,38) = 1.631,

1453 p = 0.2093, Fisher's LSD, *p £ 0.05). N = 9-12/group. **E)** Quantification of *Drd1* mRNA puncta
1454 in CA1 nuclei (Student's t-test, (t(4854) = 2.249, *p = 0.00246). **F)** Quantification of *Drd2* mRNA
1455 puncta in CA1 nuclei (Student's t-test, (t(4854) = 1.502, p = 0.1132). **G)** Quantification of *Drd1*
1456 mRNA puncta in dentate gyrus nuclei (Student's t-test, (t(11946) = 3.900, ****p < 0.0001). **H)**
1457 Quantification of *Drd2* mRNA puncta in dentate gyrus nuclei (Student's t-test, (t(11946) = 6.034,
1458 ****p < 0.0001). **I)** Schematic of working model.
1459

1460 **SUPPLEMENTAL REFERENCES**

1461 76. Rice, C. J., Sandman, C. A., Lenjavi, M. R. & Baram, T. Z. A novel mouse model for acute
1462 and long-lasting consequences of early life stress. *Endocrinology* **149**, 4892–4900 (2008).
1463 77. Gilles, E. E., Schultz, L. & Baram, T. Z. Abnormal corticosterone regulation in an
1464 immature rat model of continuous chronic stress. *Pediatr Neurol* **15**, 114–119 (1996).
1465 78. Peña, C. J. *et al.* Early life stress confers lifelong stress susceptibility in mice via ventral
1466 tegmental area OTX2. *Science* **356**, 1185–1188 (2017).
1467 79. Fleming, A. S. & Rosenblatt, J. S. Maternal behavior in the virgin and lactating rat. *Journal*
1468 *of Comparative and Physiological Psychology* **86**, 957–972 (1974).
1469 80. Krishnan, V. *et al.* Molecular Adaptations Underlying Susceptibility and Resistance to
1470 Social Defeat in Brain Reward Regions. *Cell* **131**, 391–404 (2007).
1471 81. Carcea, I. *et al.* Oxytocin neurons enable social transmission of maternal behaviour. *Nature*
1472 **596**, 553–557 (2021).
1473 82. Wolcott, N. S. *et al.* Automated classification of estrous stage in rodents using deep
1474 learning. *Sci Rep* **12**, 17685 (2022).
1475 83. Nagai, Y. *et al.* Deschloroclozapine, a potent and selective chemogenetic actuator enables
1476 rapid neuronal and behavioral modulations in mice and monkeys. *Nat Neurosci* **23**, 1157–
1477 1167 (2020).
1478 84. Secci, M. E., Reed, T., Quinlan, V., Gilpin, N. W. & Avegno, E. M. Quantitative Analysis
1479 of Gene Expression in RNAscope-processed Brain Tissue. *Bio Protoc* **13**, e4580 (2023).
1480 85. Bray, N. L., Pimentel, H., Melsted, P. & Pachter, L. Near-optimal probabilistic RNA-seq
1481 quantification. *Nature biotechnology* **34**, 525–527 (2016).
1482 86. Risso, D., Ngai, J., Speed, T. P. & Dudoit, S. Normalization of RNA-seq data using factor
1483 analysis of control genes or samples. *Nat Biotechnol* **32**, 896–902 (2014).
1484 87. Peixoto, L. *et al.* How data analysis affects power, reproducibility and biological insight of
1485 RNA-seq studies in complex datasets. *Nucleic Acids Res* **43**, 7664–7674 (2015).
1486 88. Love, M. I., Huber, W. & Anders, S. Moderated estimation of fold change and dispersion
1487 for RNA-seq data with DESeq2. *Genome Biol* **15**, 550 (2014).
1488 89. Ge, S. X., Jung, D. & Yao, R. ShinyGO: a graphical gene-set enrichment tool for animals
1489 and plants. *Bioinformatics* **36**, 2628–2629 (2020).
1490 90. Supek, F., Bošnjak, M., Škunca, N. & Šmuc, T. REVIGO Summarizes and Visualizes Long
1491 Lists of Gene Ontology Terms. *PLOS ONE* **6**, e21800 (2011).
1492 91. Krämer, A., Green, J., Pollard, J., Jr & Tugendreich, S. Causal analysis approaches in
1493 Ingenuity Pathway Analysis. *Bioinformatics* **30**, 523–530 (2014).
1494 92. Shen, L. GeneOverlap: An R package to test and visualize gene overlaps.
1495 93. Matevossian, A. & Akbarian, S. Neuronal Nuclei Isolation from Human Postmortem Brain
1496 Tissue. *J Vis Exp* 914 (2008) doi:10.3791/914.
1497 94. Hao, Y. *et al.* Integrated analysis of multimodal single-cell data. *Cell* **184**, 3573-3587.e29
1498 (2021).
1499 95. Young, M. D. & Behjati, S. SoupX removes ambient RNA contamination from droplet-
1500 based single-cell RNA sequencing data. *Gigascience* **9**, giaa151 (2020).
1501 96. McGinnis, C. S., Murrow, L. M. & Gartner, Z. J. DoubletFinder: Doublet Detection in
1502 Single-Cell RNA Sequencing Data Using Artificial Nearest Neighbors. *Cell systems* **8**,
1503 329-337.e4 (2019).

1504 97. Artegiani, B. *et al.* A Single-Cell RNA Sequencing Study Reveals Cellular and Molecular
1505 Dynamics of the Hippocampal Neurogenic Niche. *Cell Reports* **21**, 3271–3284 (2017).
1506 98. Zhou, Z., Zhi, C., Chen, D., Cai, Z. & Jiang, X. Single-nucleus RNA sequencing reveals
1507 cell type-specific transcriptome alterations of Down syndrome hippocampus using the
1508 Dp16 mouse model. *Genes Genomics* **45**, 1305–1315 (2023).
1509 99. Cembrowski, M. S., Wang, L., Sugino, K., Shields, B. C. & Spruston, N. Hipposeq: a
1510 comprehensive RNA-seq database of gene expression in hippocampal principal neurons.
1511 *eLife* **5**, e14997.
1512 100. Harris, K. D. *et al.* Classes and continua of hippocampal CA1 inhibitory neurons revealed
1513 by single-cell transcriptomics. *PLoS Biol* **16**, e2006387–e2006387 (2018).
1514 101. Haslinger, A., Schwarz, T. J., Covic, M. & Lie, D. C. Expression of Sox11 in adult
1515 neurogenic niches suggests a stage-specific role in adult neurogenesis. *Eur J Neurosci* **29**,
1516 2103–2114 (2009).
1517 102. Bandler, R. C. *et al.* Single-cell delineation of lineage and genetic identity in the mouse
1518 brain. *Nature* **601**, 404–409 (2022).
1519 103. Olney, K. C. *et al.* Widespread choroid plexus contamination in sampling and profiling of
1520 brain tissue. *Mol Psychiatry* **27**, 1839–1847 (2022).
1521 104. Xiang, M. *et al.* A Single-Cell Transcriptional Roadmap of the Mouse and Human Lymph
1522 Node Lymphatic Vasculature. *Front Cardiovasc Med* **7**, 52 (2020).
1523 105. Tasic, B. *et al.* Adult Mouse Cortical Cell Taxonomy by Single Cell Transcriptomics. *Nat*
1524 *Neurosci* **19**, 335–346 (2016).
1525 106. Miller, S. A. *et al.* LSD1 and aberrant DNA methylation mediate persistence of
1526 enteroendocrine progenitors that support BRAF mutant colorectal cancer. *Cancer Res* **81**,
1527 3791–3805 (2021).
1528
1529